BBA - Molecular and Cell Biology of Lipids 1869 (2024) 159443

Contents lists available at ScienceDirect

BBA - Molecular and Cell Biology of Lipids

journal homepage: www.elsevier.com/locate/bbalip

Interaction of ROMK2 channel with lipid kinases DGKE and AGK: Potential channel activation by localized anionic lipid synthesis

Milena Krajewska [a,1], Mariusz Możajew [a,b], Sławomir Filipek [b], Piotr Koprowski [a,*]

[a] Laboratory of Intracellular Ion Channels, Nencki Institute of Experimental Biology PAS, Warsaw, Poland
[b] Faculty of Chemistry, Biological and Chemical Research Centre, University of Warsaw, Warsaw, Poland

ARTICLE INFO

Keywords:
Protein-protein interactions
Proximity biotinylation
Potassium channel
Lipid kinase
Phosphatidic acid

ABSTRACT

In this study, we utilized enzyme-catalyzed proximity labeling with the engineered promiscuous biotin ligase Turbo-ID to identify the proxisome of the ROMK2 channel. This channel resides in various cellular membrane compartments of the cell including the plasma membrane, endoplasmic reticulum and mitochondria. Within mitochondria, ROMK2 has been suggested as a pore-forming subunit of mitochondrial ATP-regulated potassium channel (mitoK$_{ATP}$). We found that ROMK2 proxisome in addition to previously known protein partners included two lipid kinases: acylglycerol kinase (AGK) and diacylglycerol kinase ε (DGKE), which are localized in mitochondria and the endoplasmic reticulum, respectively. Through co-immunoprecipitation, we confirmed that these two kinases are present in complexes with ROMK2 channels. Additionally, we found that the products of AGK and DGKE, lysophosphatidic acid (LPA) and phosphatidic acid (PA), stimulated the activity of ROMK2 channels in artificial lipid bilayers. Our molecular docking studies revealed the presence of acidic lipid binding sites in the ROMK2 channel, similar to those previously identified in Kir2 channels. Based on these findings, we propose a model wherein localized lipid synthesis, mediated by channel-bound lipid kinases, contributes to the regulation of ROMK2 activity within distinct intracellular compartments, such as mitochondria and the endoplasmic reticulum.

1. Introduction

Mitochondria are crucial for the energy metabolism of the cell, and also play a role in regulating cell death and survival. The permeability of the inner mitochondrial membrane (IMM) is a complex process. Studies have identified the presence of ion channels in the IMM [reviewed in [1]], including the mitochondrial potassium channel regulated by ATP (mitoK$_{ATP}$). The mitoK$_{ATP}$ channel activity has been detected in various tissues, including the liver [2], heart [3], kidney [4], brain [5,6], skeletal muscle [7], and human T lymphocytes [8]. Alternatively, two different proteins ROMK2 (Kir1.1b) - a splice variant of the KCNJ1 gene product [19] or CCDC51 protein (mitoK) [9] have been proposed to be the pore-forming subunits of the mitoK$_{ATP}$ channel. Despite a considerable body of literature on the activity [8,10–13] and small-molecule regulation [14–18] of the mitoK$_{ATP}$ channel, the connection between its activity and the functioning of ROMK2 in mitochondria remains inadequately understood [19,20], and even questioned [9,21,116]. Previously, ROMK2 activity has been recorded in the plasma membrane (PM) [22,23]. Recent studies, however, have described the activity of ROMK2 also in mitochondria [20]. ROMK2 differs from its ROMK1 (Kir1.1a) isoform by the absence of the first 19 amino acids, which likely reveals the mitochondrial localization signal at the ROMK2 N-terminus [19,24]. While ROMK channels located in the plasma membrane have been shown to interact with a few accessory proteins that modulate their activity and ligand sensitivity [25–27] nothing is known about proteins that interact with the ROMK2 channel in mitochondria. Hence, the initial goal of the project was to identify protein partners of ROMK2 in the mitochondria to support the function of these channels in these organelles. To accomplish this, we employed TurboID, a variant of the proximity-dependent biotinylation (Bio-ID) method [28]. However, due to the localization of the ROMK2 variant in multiple membrane compartments and the isolation of intracellular fractions that contained various membranes, this approach has led to the detection of several proteins that were known to interact with the ROMK channel outside mitochondria. More importantly, our results also uncovered new partners to ROMK2 including acylglycerol kinase (AGK) and diacylglycerol

* Corresponding author.
E-mail address: p.koprowski@nencki.edu.pl (P. Koprowski).
[1] Current affiliation: Interdisciplinary Laboratory of Molecular Biology and Biophysics, Centre of New Technologies, University of Warsaw, Warsaw, Poland.

https://doi.org/10.1016/j.bbalip.2023.159443
Received 28 August 2023; Received in revised form 20 November 2023; Accepted 30 November 2023
Available online 4 December 2023

kinase ε (DGKE). Co-immunoprecipitation (Co-IP) experiments revealed the presence of protein complexes containing ROMK2 and AGK or DGKE. AGK is a dual-function mitochondrial enzyme that catalyzes the phosphorylation of mono- and diacylglycerols (MAGs and DAGs) to lysophosphatidic acid (LPA) and phosphatidic acid (PA) [29], and it is also a subunit of the TIM22 import complex located in the IMM [30,31]. This complex is involved in the import of a subclass of mitochondrial proteins [32]. DGKE is mainly localized in the ER [33,115]. DGKE catalyzes the phosphorylation of DAG to PA [117]. The activity of the ROMK2 channel was stimulated by LPA and PA, suggesting that localized anionic lipid synthesis by AGK and DGKE may regulate its activity in separate cell compartments.

2. Materials and methods

2.1. Chemicals

Primers for DNA amplification and sequencing were synthesized by Sigma-Aldrich. Vectors for Turbo-ID were obtained from Addgene. 3xHA-TurboID-NLS_pCDNA3 was a gift from Alice Ting (Addgene plasmid #107171; http://n2t.net/addgene:107171; RRID: Addgene_107,171) [28]. pSmac-GFP was provided by Douglas Green (Addgene plasmid #40881; http://n2t.net/addgene:40881; RRID: Addgene_40,881) [34]. pOTC was provided by Nicholas Hoogenraad (Addgene plasmid #71877; http://n2t.net/addgene:71877; RRID: Addgene_71,877) [35]. Vectors with pCMV6-Entry plasmid backbone, which express proteins with Myc-FLAG-tags (in this study referred to as FLAG tag only) for Co-IP were obtained from OriGene for the following proteins: PRDX1 (cat. no. RC205072), GPATCH8 (cat. no. RC219640), TP53 (cat. no. RC200003), IMPDH2 (cat. no. RC202977), AGK (cat. no. RC201891), PARP1 (cat. no. RC207085), DGKE (cat. no. RC219913). Phusion Hot Start II DNA polymerase and restriction enzymes were purchased from Thermo Fisher Scientific. Sequencing services for all DNA constructs were provided by Genomed (www.genomed.pl). Kits for DNA purification were purchased from EURx (Poland) and Promega (Poland). SDS-PAGE protein ladders were purchased from Thermo Fisher Scientific (cat. no. 26616, 26,625); Blue Native PAGE marker was purchased from GE Healthcare (cat. no. 17044501). The following antibodies were obtained from the indicated suppliers: anti-HA (Sigma-Aldrich, cat. no. H9658), anti-V5 (Sigma-Aldrich, cat. no. V8012), anti-KCNJ1 (Sigma-Aldrich, cat. no. HPA026962), anti-coxIV (Cell Signaling Technology, cat. no. 4844), anti-DDK (anti-FLAG) (OriGene, cat. no. TA50011), anti-AGK (OriGene, cat. no. TA344897), anti-DGKE (Proteintech, cat. no. 11900-1-AP), anti-SDHA (Abcam, cat. no. 137040), anti-alpha 1 Sodium Potassium ATPase (Abcam, cat. no. 7671), anti-TOMM20 (Sigma Aldrich, cat. no. HPA011562), anti-TIMM29 (Origene, cat. no. CF11979), anti-Calnexin (Abcam, cat. no. 219644), anti-EEA1 (Abcam, cat. no. 206860), Alexa Fluor 555 anti-rabbit IgG (Invitrogen, cat. no. A31572), Alexa Fluor 488 anti-mouse IgG (Invitrogen, cat. no. A21202), Alexa Fluor 555 anti-mouse IgG (Invitrogen, cat. no. A31570), Alexa Fluor 488 anti-rabbit IgG (Invitrogen, cat. no. A11008), Alexa Fluor 405 anti-goat IgG (Abcam, cat. no. 175665). Streptavidin-HRP was purchased from Thermo Fisher Scientific (cat. no. 21130). V5-tagged Protein Magnetic Purification Kit (cat. no. 3341) and DDDDK (FLAG)-tagged Protein Magnetic Purification Kit (cat. no. 334R) for co-immunoprecipitation were purchased from MBL, Life Science. Dynabeads™ Antibody Coupling Kit (cat. no. 14311D) was obtained from Invitrogen. Diisobutylene-maleic acid copolymer – DIBMA (brand name Sokalan® CP9) was a gift from BASF (Poland). Styrene-maleic acid copolymers - SMA (brand name XIRAN®) of different molar ratios: SMA 1.2:1, SMA 2.3:1, and SMA 3:1 were a gift from Polyscope (Netherlands). ATP/Mg^{2+} was obtained from Sigma Aldrich (cat. no. A9187), and VU591 was purchased from Alomone Labs (cat. no. V-125). Oleoyl-L-α-lysophosphatidic acid sodium salt (LPA) was obtained from Sigma Aldrich (cat. no. L7260), while 1-palmitoyl-2-oleoyl-sn-glycero-3-phosphate sodium salt (PA) was obtained from Avanti® Polar Lipids (cat. no. 840857). All other chemicals and materials were purchased from Sigma-Aldrich, Roche Diagnostics, Bio-Rad Laboratories, or GE Healthcare unless otherwise indicated.

2.2. Plasmids construction

For proximity biotinylation experiments pcDNA3.1/Hygro(+) vectors carrying the open reading frames encoding TurboID-3xHA fusion proteins were constructed. To create the construct expressing ROMK2-TurboID-3xHA three-step overlap extension PCR approach was used. In the first step, three PCR reactions were performed in parallel as follows. In reaction #1 fragment encoding ROMK2 was amplified using pcDNA3.1-ROMK2-V5 plasmid as a template and primers: GA1_up, 5'-**TGGAATTCTGCAGAT**ATGTTCAAACATCTTCGGAAATGGG-3′ (bold - sequence homologous to MCS sequence of pcDNA3.1/Hygro(+), underlined - sequence encoding ROMK2) and GA1_lw, 5'-**TTGCTAGCCAT**TTTGGTGTCATCTGTTTCA-3′ (bold - sequence encoding linker, underlined - sequence encoding ROMK2). In reaction #2 fragment encoding TurboID was amplified using the 3xHA-TurboID-NLS_pCDNA3 plasmid as a template and primers GA2_up, 5'-**CCAAAATGGCTAGC**AAAGACAATACTGTGCC-3′ (bold - sequence of the linker, underlined - sequence encoding TurboID) and GA2_lw, 5'-**TACGGGTAGAA**TTCCTTTTCGGCAGACCG-3′ (bold - sequence encoding 3xHA-tag, underlined - sequence encoding *TurboID*). In reaction #3 fragment encoding 3xHA-tag was amplified using the 3xHA-TurboID-NLS_pCDNA3 plasmid as a template and primers GA3_up, 5'-AGGAA**TTCTACCCGTATGATGTTCCGGA**-3′ (bold - 5` sequence encoding 3xHA-tag, underlined - sequence encoding TurboID) and GA3_lw 5'-GCCACTGTGCTGGA**TTTATGCGTAGTCTGGGACGTC**-3′ (bold - 5` sequence of the 3xHA-tag). The products of the first-step reactions (#1, #2, #3) were purified from the agarose gel (Agarose-Out DNA purification kit, EURx, E3540). In the second step, the products of reactions #1 and #2 were used together with primers GA1_up and GA2_lw to obtain the fragment encoding the ROMK2-TurboID fusion. The product of this reaction was gel purified and used with product #3 in subsequent PCR with primers: upper 5'-GAGCTC**GGATCC**ATGTTCAAACATCTTCGGAAATG-3′ (bold - sequence recognized by BamHI, underlined - sequence encoding ROMK2) and lower 5'-TCTAGA**CTCGAG**TTATGCGTAGTCTGGGA-3′ (bold - sequence recognized by *Xho*I, underlined - sequence encoding 3xHA-tag) to obtain fragment encoding ROMK2-TurboID-3xHA fusion. In the expressed fusion protein, the ROMK2 sequence is directly followed by TurboID-3xHA, meaning that the signal encoding nuclear localization signal (NLS) present in the original plasmid 3xHA-TurboID-NLS_pcDNA3.1 is missing (Sup. Fig. 1). To create a construct expressing SMAC-TurboID-3xHA fusion two-step PCR approach was used. In the first step, the SMAC leader sequence was amplified by PCR with the pSmac-GFP template using primers: upper 5'-ATG**GGATCC**ATGGCGGCTCTGAAGAGTTGG-3′ (bold - sequence recognized by BamHI, underlined - sequence encoding SMAC leader) and lower 5'-**CAGAGGCACAGTATTGTCTTT**CATAATAGGAACCGCACACAGGGTTAC-3′ (bold - sequence sequence encoding TurboID, underlined - sequence encoding SMAC leader). In the second step, the first-step PCR product was used as the forward "megaprimer" [36] with the reverse primer 5'-TCTAGA**CTCGAG**TTATGCGTAGTCTGGGA-3′ (bold - sequence recognized by *Xho*I, underlined - sequence encoding 3xHA) and the pcDNA3.1-ROMK2-TurboID plasmid as the template to obtain fragment encoding SMAC-TurboID-3xHA fusion (Sup. Fig. 2). To create a construct expressing OTC-TurboID-3xHA fusion similar two-step PCR approach was also used. In the first step, the OTC leader sequence was PCR amplified with the pOTC plasmid as the template using primers forward 5'-ATG**GGATCC**ATGCTGTCTAATTTGAGAATCCTGCTC-3′ (bold - sequence recognized by BamHI, underlined - sequence encoding OTC leader) and reverse 5'-**GCTTCAGAGGCACAGTATTGTCTTT**CTGGACTGGCTTCCCATACC-3′ (bold - sequence sequence encoding TurboID, underlined - sequence encoding OTC leader). The second step reaction was performed as described above for the SMAC fusion construct to obtain fragment

encoding OTC-TurboID-3xHA fusion (Sup. Fig. 3).

All the final PCR products, i.e. ROMK2-TurboID-3xHA, SMAC-TurboID-3xHA, and OTC-TurboID-3xHA were digested with BamHI and *Xho*I restriction enzymes and then cloned into pcDNA3.1/Hygro(+) vector linearized with BamHI and XhoI enzymes, whereby the pROMK2-TurboID-3xHA, pSMAC-TurboID-3xHA, and pOTC-TurboID-3xHA vectors were generated.

The pROMK2-V5 vector was created by ligation of the *Kpn*I and *Xho*I digested ROMK2-V5 with pcDNA3.1/Hygro(+) linearized with the same enzymes. ROMK2-V5 was obtained by PCR with pCMV-ROMK2-eGFP plasmid as the template [19] using primers: forward 5'-ACT**GGTAC-C**ATGTTCAAACATCTTCGGAAATGG-3′ (bold - sequence recognized by KpnI, underlined - sequence encoding ROMK2, and reverse 5'-CGG**CTCGAG**TTACGTAGAATCGAGACCGAGGAGAGGGTTAGGGA-TAGGCTTACCCATTTTGGT GTCATCTG-3′ (bold - sequence recognized by XhoI, underlined - sequence encoding V5 tag, double underlined - sequence encoding ROMK2).

All the above-described constructs were verified by sequencing.

Vectors carrying the ORFs encoding AGK-FLAG, p53-FLAG, GPATCH8-FLAG, PRDX1-FLAG, IMPDH2-FLAG, PARP1-FLAG, and DGKE-FLAG were propagated in *E. coli* CopyCutter ™ EPI400 ™ strain (Biosearch Technologies, cat. no. C400CH10) according to producer instructions. Briefly, an overnight culture (5 ml of LB with antibiotic) was prepared by inoculation with a single colony or 10 μl of a transformation reaction and then shaking overnight at 37 °C. The overnight culture was diluted at 1:10 and the OD at 600 nm was measured (OD_{600}), then the overnight culture was diluted to a final OD_{600} value of 0.2 in 250 ml of LB supplemented with antibiotic and 0.25 ml of 1000× CopyCutter™ Induction Solution (Biosearch Technologies, cat. no. CIS40025). The resulting mixture was then incubated at 37 °C for 4 h with vigorous shaking, and then plasmid DNA was isolated (PureYield™ Plasmid Maxiprep System, Promega, cat. no. A2393). All other vectors were propagated in *E. coli* NEB® Stable cells (New England BioLabs, cat. no. C3040H). Plasmid DNA was isolated with the PureYield™ Plasmid Maxiprep System (Promega, cat. no. A2393).

2.3. Cell culture

HEK293T cells were cultured at 37 °C under 5 % CO_2 in Dulbecco's Modified Eagle Medium (DMEM) (Laboratory of General Chemistry, Ludwik Hirszfeld Institute of Immunology and Experimental Therapy, Polish Academy of Sciences) supplemented 10 % (vol/vol) fetal bovine serum (FBS) (Gibco, cat. no. A4766801), 2 mM L-glutamine (Biowest, cat. no. X0550), 100 units/ml penicillin, and 100 μg/ml streptomycin (Sigma Aldrich, cat. no. P0781).

2.3.1. Cells transfection

For transient expression, HEK293T cells with confluency of about 60–80 % were transfected using polyethyleneimine (PEI, Sigma Aldrich, cat. no. 408727). The experiments were carried out with cell cultures grown in 150 mm Petri dishes with 5–10 Petri dishes per sample for the TurboID experiment, and 2 dishes per sample for the Co-IP experiment.

To determine the optimal transfection conditions in TurboID experiments, cells grown in 6-well plates were transfected with varying amounts of DNA (0.5 and 2.5 μg) and PEI to DNA ratios (2:1, 4:1, and 8:1). The optimal transfection conditions were determined to be 2.5 μg of DNA and 4:1 PEI to DNA ratio.

For final TurboID experiments, the transfection mixture was prepared by mixing 860 μl of OPTIMEM (Opti-MEM® I Reduced Serum Medium, Gibco, cat. no. 11058–021), 10.75 μg of DNA (pcDNA3.1, pSMAC-TurboID-3xHA, pOTC-TurboID-3xHA or pROMK2-TurboID-3xHA) and 43 μg PEI and incubating for 15 min. This mixture was then added to the Petri dishes containing cell cultures growing in fresh DMEM supplemented with 10 % (vol/vol) FBS and 2 mM L-glutamine.

To optimize cell transfection in Co-IP experiments cells growing in 6-well plates were transfected with the pROMK2-V5 plasmid. Two DNA amounts (0.5 and 2.5 μg), and three different PEI:DNA ratios (2:1, 4:1, and 8:1) were used. The optimal conditions were identified as 2.5 μg of DNA and a 4:1 PEI:DNA ratio. Next, transfection efficiency with the pCMV6-Entry series of plasmids was optimized using a constant amount of 2.5 μg DNA and three different PEI:DNA ratios (2:1, 4:1, and 8:1). The optimal ratio of 4:1 was used in subsequent experiments. For the Co-IP experiments, cells were transfected with the plasmid pROMK2-V5 and one of the pCMV6-Entry series of plasmids containing the sequence coding a potential interaction protein, i.e. AGK-FLAG, p53-FLAG, GPATCH8-FLAG, IMPDH2-FLAG, PRDX1-FLAG, PARP1-FLAG, and DGKE-FLAG. The transfection mix consisted of 860 μl of OPTIMEM (Opti-MEM® I Reduced Serum Medium, Gibco, cat. no. 11058–021), 10.75 μg of the pROMK2-V5 plasmid, 10.75 μg of pCMV6-Entry plasmid, and 86 μg of PEI. The mixture was incubated for 15 min at room temperature and then added to the cells. Controls for the Co-IP experiments included transfecting the cells only with the pROMK2-V5 plasmid or with pCMV6-Entry plasmid (DNA 10.75 μg; PEI:DNA ratio was 4:1), as well as using untransfected HEK293T cells or cells transfected with pcDNA3.1.

For immunofluorescence, 150,000 cells were plated on a 35 mm glass-bottom dish (Cellvis). Cells were transfected with 2.5 μg of DNA (TurboID: pcDNA3.1, pSMAC-TurboID-3xHA, pOTC-TurboID-3xHA or pROMK2-TurboID-3xHA; Co-IP: pROMK2-V5 and/or pAGK-FLAG, pROMK2-V5 and/or pDGKE-FLAG*)* or 1.5 μg of DNA for analysis of compartment in with which collocation is observed and PEI:DNA ratio 4:1 in 200 μl OPTIMEM.

2.3.2. In vivo biotinylation

To optimize biotinylation conditions cells transfected with pSMAC-TurboID-3xHA, pOTC-TurboID-3xHA, or pROMK2-TurboID-3xHA plasmids were treated with two biotin concentrations (50 and 500 μM) and analyzed for protein biotinylation. In the case of pROMK2-TurboID-3xHA plasmid, different biotinylation times (20 min, 1 h, and 3 h) were also assessed. Three-hour biotinylation time was used in subsequent experiments.

In TurboID experiments, 24 h after transfection medium was replaced with DMEM supplemented with FBS and L-glutamine, and 500 μM biotin (50 μM biotin was used in one experiment). The cultures were then incubated at 37 °C for 3 h in 5 % CO_2 environment. The cells were washed twice with PBS to remove excess biotin, detached mechanically, and harvested by centrifugation for 10 min at 800 xg. The cell pellet was frozen in liquid nitrogen and stored at −80 °C for further use.

2.3.3. Isolation of mitochondria-enriched fraction

Mitochondria-enriched fractions were isolated using two different protocols depending on their intended use. For the TurboID experiments, the mitochondria-enriched fractions were prepared according to the previously described protocol [37] with modifications. Cell pellet (300–500 mln cells) was resuspended in 16 ml of Isolation Buffer (IB) containing 210 mM mannitol, 70 mM sucrose, 500 mM HEPES/KOH (pH 7.2), 0.25 % Bovine Serum Albumin (BSA), Complete Protease Inhibitor Cocktail (cOmplete™, Roche, cat. no. 11873580001), and 1 mM phenylmethylsulfonyl fluoride (PMSF). Then digitonin was added to the final concentration of 200–400 ng/μl to permeabilize the cells by 80–90 %. Next, the sample was diluted to a final volume of 50 ml with IB and centrifuged at 3000 xg for 10 min at 4 °C. The resulting thick, white, gelatinous pellet was suspended in 15 ml IB with BSA and homogenized. Centrifugations were performed at 1200 x g for 10 min at 4 °C until the pellet was no longer visible (about 3 times). The final supernatant was centrifuged at 10,000 xg for 1 h at 4 °C. The resulting pellet was suspended in 5 ml IB and centrifuged (10,000 xg, 4 °C, 30 min). After centrifugation, the supernatant was discarded leaving a brown pellet containing the mitochondria. The resulting pellet containing mitochondria was resuspended in 1 ml IB and centrifuged at 10,000 xg at 4 °C for 15 min, followed by two repetitions.

The mitochondria-enriched fraction for experiments with SMA (poly

[styrene-*co*-(maleic acid)]) and DIBMA (poly[diisobutylene-*alt*-(maleic acid)]) was isolated according to a previously published protocol [38]. Cells were thawed on ice and resuspended in 10 ml of 250 mM sucrose in SIB buffer containing 1 mM EGTA, 5 mM HEPES/KOH (pH 7.2) supplemented with protease inhibitors cOmplete™ (Roche, cat. no. 11873580001) and PMSF (1 mM). Cells were homogenized and centrifuged at 9200 x*g* for 10 min at 4 °C. The resulting pellet was suspended in 5 ml SIB buffer and centrifuged at 800 x*g* for 20 min at 4 °C. The supernatant containing the mitochondria was transferred to a new Falcon tube and centrifuged at 9200 x*g*, 4 °C for 10 min. The pellet was resuspended in 1 ml SIB buffer and centrifuged again in the same conditions. This centrifugation was repeated twice. The pellet containing the mitochondria was used immediately or resuspended in a small amount of storage buffer (150 mM KCl, 10 mM HEPES/KOH, pH 7.2), aliquoted into portions of 10 µl, and stored at −80 °C.

2.4. Protein isolation and purification

The protein purification procedure in TurboID experiments was performed as described previously [39], with slight modifications. A mitochondria-enriched fraction was resuspended in 5 ml of TurboID Lysis Buffer (TLB) containing 150 mM NaCl, 0.4 % SDS, 1 % NP-40, 1 mM EGTA, 1.5 mM $MgCl_2$, 50 mM Tris (pH 7.4), 1 mM PMSF, and protease inhibitors cOmplete™ (Roche, cat. no. 11873580001). The sample was then sonicated on ice for 2 min using Digital Sonifier 250 (Branson Ultrasonic Corporation) with a 50 % duty cycle. After sonication 9 ml of TLB was added and then the sample was mixed for 10 min at 4 °C, followed by centrifugation at 5500 x*g* for 30 min at 4 °C. The supernatant was transferred to a new Falcon tube and mixed with magnetic streptavidin beads (Dynabeads® MyOne™ Streptavidin C1, ThermoScientific, cat. no. 65002) pre-equilibrated with the TLB buffer. The sample was slowly mixed overnight in a rotator at 4 °C. The next day, the solution was removed from the beads by magnetic separation and then the resin was washed twice for 10 min with 5 ml TurboID Wash Buffer 1 (TWB1: 2 % SDS, 50 mM Tris, pH 7.4). Then the resin was washed in the same manner with the following buffers: TurboID Wash Buffer 2 (TWB2: 0.1 % sodium deoxycholate, 1 % Triton X-100, 1 mM EDTA, 500 mM NaCl, 50 mM HEPES/NaOH, pH 7.5) and TurboID Wash Buffer 3 (TWB3: 5 % sodium deoxycholate, 0.5 % NP-40, 1 mM EDTA, 250 mM LiCl, 10 mM Tris, pH 7.4). Additionally, the resin was washed 7–10 times with 5 ml of 10 mM Tris, pH 7.4. Finally, the resin was resuspended in 100 µl of 10 mM Tris, pH 7.4. Proteins retained on the magnetic beads were analyzed by mass spectrometry. Additionally, proteins were also eluted from the resin by incubation for 10 min at 95 °C in 2× Laemmli Sample Buffer (BioRad) supplemented with 5 mM biotin [40] and analyzed by SDS-PAGE/Western Blot.

For Co-IP experiments, cells were transfected/co-transfected with plasmids pROMK2-V5 and/or pPRDX1-FLAG, pGPATCH8-FLAG, pTP53-FLAG, pIMPDH2-FLAG, pAGK-FLAG, pPARP1-FLAG, pDGKE-FLAG. After 24 h post-transfection cells were washed two times with PBS, collected, and centrifuged at 800 x*g* for 10 min at 4 °C. Next, 1 ml of Co-IP Lysis Buffer (1 % Triton X-100, 5 mM EDTA, 150 mM NaCl, 20 mM Tris, pH 7.5, protease inhibitor cocktail cOmplete™ - Roche, cat. no. 11873580001, and 1 mM PMSF) was added to the cells pellet and the sample was mixed for 20 min at 4 °C. After this time sample was centrifuged at 15,000 ×*g* for 15 min at 4 °C. The supernatant was divided into two equal parts. One part was used to purify FLAG-tagged proteins with DDDDK-tagged Protein Magnetic Purification Kit (MBL, Life Science, cat. no. 3343R), and the second part was used to purify V5-tagged proteins with V5-tagged Protein Magnetic Purification Kit (MBL, Life Science, cat. no. 3341) according to the manufacturer protocol, with minor changes. Briefly, before use, magnetic beads were rinsed three times with the Co-IP Wash Buffer (300 mM NaCl, 0.1 % Tween-20, 20 mM Tris, pH 7.5) and then once with Co-IP Lysis Buffer. After equilibration 50 µl of magnetic beads were added to the sample and incubated at 4 °C for 1 h with gentle mixing. Next, the unbound material was removed, and the resin was rinsed 10 times with 1 ml Co-IP Wash Buffer. The resin was suspended in 40 µl of peptide solution (2 mg/ml of V5-tag peptide or 1 mg/ml of DDDDK peptide) and then incubated for 10 min at room temperature. After separation from the beads, the elution fraction was mixed with 1× Laemmli Sample Buffer and analyzed by SDS-PAGE/Western Blot.

Co-IP experiments between ROMK2-V5 and AGK-FLAG or DGKE-FLAG proteins were also carried out on the anti-KCNJ1 resin. The anti-KCNJ1 resin was prepared using Dynabeads Antibody Coupling Kit (Invitrogen, cat. no. 14311D). For one experiment (4 samples), 5 mg of beads were washed with 1 ml of Dynabeads C1 Buffer. Next, 50 µl of 0.1 mg/ml anti-KCNJ1 antibody (Sigma-Aldrich, cat. no. HPA026962), 200 µl of Dynabeads Buffer C1, and 250 µl of Dynabeads Buffer C2 were added, and then beads were incubated with gentle mixing at 37 °C for around 24 h. After this time beads were washed with 800 µl of Dynabeads LB Buffer, 4 times with 800 µl Dynabeads SB. Then the buffer was removed and beads were washed with Co-IP Wash Buffer, equilibrated with Co-IP Lysis Buffer, and then resuspended in 400 µl of Co-IP Lysis Buffer. For one sample 1.25 mg of beads were used, i.e. 100 µl of beads was added to each sample. The further procedure was carried out as described above.

The interaction of ROMK2-V5 with AGK-FLAG or DGKE-FLAG proteins was also investigated after protein solubilization in polymer (native) nanodiscs. To find optimal conditions for copolymer solubilization mitochondria were isolated from HEK293T cells transfected with pROMK2-V5 and then solubilized with 2.5 % SMA (3:1; 2.3:1 and 1.2:1) (Polyscope Polymers, The Netherlands) or 2.5 % DIBMA (BASF, Poland). Solubilization was performed for 4 h at 25 °C in Polymer Solubilization Buffer (PSB: 200 mM KCl, 1 mM EDTA, 50 mM Tris, pH 7.4, 1× cOmplete™ protease inhibitors (Roche, cat. no. 11873580001), 1 mM PMSF). After that time, the sample was centrifuged at 15,000 x*g* for 20 min at 4 °C to remove the insoluble fraction. Pellets and supernatants were analyzed by SDS-PAGE and immunoblotting. After optimizing the solubilization conditions, HEK293T cells co-transfected with the plasmids expressing ROMK2-V5 and AGK-FLAG or DGKE-FLAG were solubilized overnight with gentle shaking in the PSB buffer containing 2.5 % DIBMA. The next day, the mixture was passed 3–5 times through a thin needle and centrifuged for 20 min at 15,000 x g at 4 °C. The supernatant was divided into two equal parts: one was used to purify FLAG-tagged proteins with the DDDDK-tagged Protein Magnetic Purification Kit (MBL, Life Science, cat. no. 3343R) and the second part was used to purify V5-tagged proteins with the V5-tagged Protein Magnetic Purification Kit (MBL, Life Science, cat. no. 3341) according to manufacturer protocol with changes. Briefly, magnetic beads were washed three times with 5 ml of Polymer Wash Buffer (PWB: 200 mM KCl, 50 mM Tris, pH 7.4) and then equilibrated with PSB with 2.5 % DIBMA. After equilibration, 50 µl of the magnetic beads were added to the supernatant. The sample was incubated with the beads for 1 h at 4 °C with gentle mixing. After this time, the unbound fraction was removed and beads were washed 10 times with 1 ml PWB buffer. After the final wash, the resin was resuspended in 40 µl of the peptide solution (2 mg/ml of V5-tag peptide or 1 mg/ml of DDDDK peptide) and then incubated for 10 min at room temperature. In the case of samples in which cells were co-transfected with pROMK2-V5 and pAGK-FLAG plasmids after separation from the beads, 10 µl of each elution fraction was taken for Western blot analysis, and 30 µl was subjected to further purification. A sample previously purified against the anti-V5 antibody was purified in the second step using the DDDDK-tagged Protein Magnetic Purification Kit (MBL, Life Science), and vice versa (i.e. a sample purified against the anti-FLAG antibody was purified using the V5-tagged Protein Magnetic Purification Kit (MBL, Life Science)). The procedure was identical to that described above.

Nanodiscs containing ROMK2-V5 protein were also immunopurified with an immobilized anti-KCNJ1 IgG antibody (Sigma Aldrich, HPA026962). The resin for this experiment was prepared as mentioned above. However, PSB containing 2.5 % DIBMA and PWB Buffers were

used for resin equilibration.

2.5. Polymer nanodiscs containing ROMK2-6xHis protein

The preparation of ROMK2-6xHis protein solubilized in polymer nanodiscs was described previously [41]. Briefly, bacterial membranes containing ROMK2-6xHis proteins were solubilized with 2.5 % SMA 2.3:1 in a buffer containing 200 mM KCl, 1 mM EDTA, 50 mM Tris/HCl, pH 7.4, and protease inhibitors (cOmplete™, Roche, cat. no. 11873580001;1 mM PMSF). The suspension was incubated overnight at 25 °C with gentle mixing and then centrifuged at 100,000 x*g* for 1 h at 4 °C. The supernatant was subjected to purification by nickel affinity chromatography (His-Select® Nickel Affinity Gel, Sigma Aldrich, cat. no. P6611). The nanodiscs containing ROMK2 protein were eluted with 250 mM imidazole. Next, native nanodiscs containing ROMK2 protein were dialyzed using a 3.5 kDa NMWCO dialysis membrane (Pierce, cat. no. 63552) against the buffer containing 300 mM KCl and 50 mM Tris/HCl, pH 7.4.

2.6. SDS-PAGE

For SDS-PAGE all samples were mixed with 4× Laemmli Sample Buffer (BioRad, cat. no. 1610747) containing 10 mM DTT and 1 mM PMSF (final concentrations) and then heated at 95 °C for 15 min. For protein elution in the Co-IP experiments in which DIBMA copolymer or anti-KCNJ1 resin was used, magnetic beads were mixed with 4× Laemmli Sample Buffer containing 10 mM DTT and 1 mM PMSF and then heated at 37 °C for 1 h.

All samples were separated in 10 % SDS-PAGE at RT. Two protein standards PageRuler™ Prestained Protein Ladder (Thermo Fisher Scientific, cat. no. 26616) and Spectra™ Multicolor High Range Protein Ladder (Thermo Fisher Scientific, cat. no. 26625) were used.

2.7. Blue native PAGE

For electrophoresis elution samples were mixed 1:10 with 10× loading dye (5 % Coomassie Blue G, 500 mM ε-amino-n-caproic acid, 100 mM Bis-Tris, pH 7.0). Samples were loaded on 4–10 % gradient blue native polyacrylamide gels and separated at 4 °C along with a molecular weight marker (GE Healthcare HMW Native Marker Kit, cat. no. 17044501).

2.8. Immunoblotting

SDS- or Blue Native-gels were electrotransferred onto Immun-Blot® polyvinylidene difluoride (PVDF) membranes (Bio-Rad, cat. no. 1620177). The membranes were immunoprobed with primary antibodies against selected proteins.

The fusions of TurboID-3xHA were detected with the anti-HA primary antibody (1:1000). Streptavidin-HRP (1:40,000) was used for the detection of biotinylated proteins. For detections of proteins in Co-IP experiments membranes were blocked with 10 % (wt/vol) milk in PBST (anti-FLAG, anti-AGK, anti-TIMM29) or TBST (anti-V5, anti-KCNJ1) or with 5 % BSA in PBST (anti-DGKE) for 2 h at RT, and then incubated overnight with anti-V5 (1:1000), anti-Flag (1:1000), anti-KCNJ1 (1:200), anti-AGK (1:500), anti-DGKE (1:500) or anti-TIMM29 (1:500) antibodies. The next day, membranes were incubated for 1 h with an appropriate secondary antibody (anti-mouse for anti-V5, anti-TIMM29, and anti-rabbit for anti-FLAG, anti-AGK, anti-DGKE, and anti-KCNJ1) linked to horseradish peroxidase (HRP). Proteins were detected by chemiluminescence (ECL Prime Western blotting detection reagent, GE Healthcare) captured on X-ray films (Amersham Hyperfilm™ ECL, GE Healthcare).

2.9. Immunofluorescence microscopy

To detect TurboID-3xHA fusions, cells were fixed with 4 % paraformaldehyde (PFA, Cell Signaling, 47746S) in PBS for 20 min, and then permeabilized by incubation in PBS buffer containing 0.05 % Triton X-100 (twice for 3 min). Next, cells were incubated overnight at 4 °C with the anti-HA and anti-TOMM20 antibodies (diluted 1:200 and 1:500, respectively, in PBS containing 4 % FBS). The next day, cells were washed three times for 8 min with PBS and then incubated for 2 h at RT with secondary antibodies anti-mouse Alexa488 (Invitrogen) and anti-rabbit IgG-Alexa555 (Invitrogen) (1:1000 each). Cells were then washed three times for 5 min with PBS and then fixed with VECTASHIELD® Antifade Mounting Media (VectorLaboratories, cat. no. H-1000-10).

Cells transfected with the pROMK2-V5 plasmid were washed in PBS buffer, incubated for 20 min in 100 nM MitoRed (Sigma Aldrich, 53,271) in FluoroBrite™ DMEM (Gibco, A1896701), and washed three times with PBS. Cells were then fixed by 20 min incubation in 4 % PFA (Cell Signaling, 47746S) in PBS and permeabilized by incubation twice for 3 min in the PBS buffer containing 0.05 % Triton X-100. Then, cells were incubated overnight with the anti-KCNJ1 antibody (1:200, Sigma Aldrich) in PBS buffer with 4 % FBS. The next day, cells were washed three times for 8 min with PBS and incubated for 2 h at RT with a secondary anti-rabbit IgG-Alexa488 antibody (1:1000, Invitrogen) in PBS buffer with 4 % FBS. After this time, cells were washed three times for 5 min with PBS and then fixed with Vectashild VECTASHIELD® Antifade Mounting Media (VectorLaboratories, cat. no H-1000-10). Additionally, the cells transfected with the pROMK2-V5 plasmid were also labeled with anti-V5 (1:200, Sigma Aldrich) and anti-coxIV (1:200, Cell Signaling) antibodies. In this case, anti-mouse IgG-Alexa488 (1:1000, Invitrogen) and anti-rabbit IgG-Alexa555 (1:1000, Invitrogen) as secondary antibodies were used. In the preparation of cells co-transfected with the pROMK2-V5 and pAGK-FLAG plasmids, the procedure was performed as mentioned above with anti-KCNJ1 (1:200, Sigma Aldrich) and anti-FLAG (1:200, Origene) antibodies in conjunction with respective secondary antibodies: anti-rabbit IgG-Alexa555 (1:1000, Invitrogen) and anti-mouse IgG-Alexa488 (1:1000, Invitrogen).

Cells co-transfected with the pROMK2-V5 and pDGKE-FLAG plasmids were stained with anti-V5 (1:200, Sigma-Aldrich) and anti-DGKE (1:500, Proteintech) antibodies in conjunction with respective secondary antibodies: anti-mouse IgG-Alexa488 (1:1000, Invitrogen) and anti-rabbit IgG-Alexa555 (1:1000, Invitrogen). In addition, these samples were stained with either anti-Calnexin (1:200, Abcam) or anti-EEA1 (1:1000, Abcam) antibody followed by secondary antibody anti-goat IgG-Alexa Fluor 405 (1:1000, Abcam).

Cell imaging was performed using an Olympus FV1200 confocal microscope running FLUOVIEW FV1000 4.2.1.20 software. Fluorescence was excited at 473 and 599 nm. All images were taken using the same confocal settings and processed using ImageJ software. Pearson's correlation coefficient (PCC) was calculated using the Fiji ImageJ with the BIOP JaCoP module, and the threshold was calculated using the Otsu algorithm.

2.10. Mass spectrometry

Biotinylated proteins isolated with magnetic streptavidin beads were analyzed by the Mass Spectrometry Laboratory at the Institute of Biochemistry and Biophysics, Polish Academy of Sciences.

MS spectra were searched against the *Homo sapiens* MassScot protein sequence database. Precursor mass tolerance was 5 ppm. Product ions were searched with a mass tolerance of 0.01 Da. The maximum precursor ion charge state used for searching was 7. The methylation of cysteines was searched as a fixed modification, while the oxidation of methionines was searched as a variable modification. The enzyme was set to trypsin in a specific mode and a maximum of one missed cleavage was allowed for searching. The following significance thresholds ($p<$)

for protein identification were specified. In the case of the control experiments, the values ranged from 0.00004489 to 0.05. For OTC, the thresholds varied from 0.0002477 to 0.02069, while for SMAC, they fell between 0.0003908 and 0.05. As for ROMK2, the threshold values spanned from 0.000133 to 0.05.

The UniProt (www.uniprot.org), the Human Protein Atlas (www.proteinatlas.org), and MitoCarta3.0 (www.broadinstitute.org/files/shared/metabolism/mitocarta/human.mitocarta3.0.html) databases were used for designations subcellular location of identified candidate proteins.

The Cytoscape with STRING database was utilized for visualizing protein interaction clusters.

2.11. Planar lipid bilayer recordings

Planar Lipid Bilayer (PLB) experiments were performed as described previously [41]. All measurements were carried out at room temperature. Lipid bilayers were formed by painting azolectin (25 mg/ml dissolved in n-decane; L-α-phosphatidylcholine from soybeans, Type II-S, Sigma Aldrich) on ~250 μm aperture in the wall of a Delrin cup (Warner Instrument Corp., Hamden, CT USA) separating two chambers (1 ml of internal volume each). The current was measured using a bilayer membrane amplifier (BLM-120, BioLogic). The formation of the lipid bilayer was monitored by the capacitance measurement feature of the amplifier. The typical capacitance of the bilayer was 70–140 pF. The electrical connections were made by agar salt bridges (3 M KCl) and Ag/AgCl electrodes. The *trans* compartment was grounded and voltage was applied to the *cis* compartment. The signal sampling frequency was 500 kHz. The conversion of the electrical signal from analog to digital was performed using a PowerLab 2/20 converter (ADInstruments). Chart v5.2.7 (PowerLab, ADInstruments) software was used to save the obtained data.

All measurements were made in the gradient system, where *cis* and *trans* compartments contained, 50 and 150 mM KCl solution, respectively. The solutions were buffered at pH 7.4 with 10 mM 4-(2-hydroxyethyl)-1-piperazine ethanesulfonic acid (HEPES). Nanodiscs containing ROMK2-6xHis protein were added to the *trans* compartment followed by gentle stirring until the channel activity was observed.

Channel modulators were added simultaneously to *cis* and *trans* compartments. ATP/Mg^{2+} (Sigma Aldrich, cat. no. A9187) was added to the final concentration of 500 μM, VU591 (6-nitro-2-[(6-nitro-1H-benzimidazol-2-yl)methoxymethyl]-1H-benzimidazole, Alomone labs, cat. no. V-125) was added to the final concentration of 20 μM. Oleoyl-L-α-lysophosphatidic acid sodium salt (LPA, Sigma Aldrich, L7260) was added to the final concentration of 100 nM; 1-palmitoyl-2-oleoyl-*sn*-glycero-3-phosphate (sodium salt), (PA, Avanti® Polar Lipids, 840,857) was added to the final concentration of 50 μg/ml.

Before analysis, all recordings were filtered at 100 Hz. The probability of channel opening (nP(o), open probability) was determined using the Clampfit 10.2 software. In figures showing channel recordings, "-" indicates the closed state of the channel. Statistical data were analyzed using Excel 2016 and Origin 2019 (OriginLab Corp.). The experimental data are reported as mean values ± standard deviations (SD). Statistical significance was determined by a paired sample Student's *t*-test and one-way ANOVA. A value of $p < 0.05$ was considered statistically significant (* $p < 0.05$; ** $p < 0.01$; *** $p < 0.001$; **** $p < 0.0001$).

2.12. Molecular modeling and docking

The homology model of ROMK2 open conformation was created using the Swiss Model service (https://swissmodel.expasy.org) [42] based on Kir2.2 K62W mutant structure (PDB ID:5kuk) as a template [43], which was the best possible template in terms of resolution (2.00 Å) and homology. Model to template similarity level was 47 %, and its structure was less certain only in the extracellular ends and the linkers connecting the membrane domain and cytoplasmic domain. The obtained structure was used to build the complex with phosphatidylinositol 4,5-bisphosphate (PIP2) in the POPC (1-palmitoyl-2-oleoyl-sn-glycero-3-phosphocholine) membrane. Four PIP2 molecules bound to ROMK2 were prepared based on the structure of chicken Kir2.2 channel with bound PIP2 (PDB ID:3SPI) (resolution 3.31 Å) [44]. The hydrophobic chains of PIP2, not visible in full in the crystal of the 3SPI structure, were extended. For this purpose, 10 carbon atoms for the stearoyl chain, and 12 carbon atoms with four double bonds for the arachidonoyl chain were added. The periodic box was set to 112.25 Å × 112.25 Å × 126.7 Å and then the POPC membrane was added using the Membrane Builder plugin in VMD 1.9.3 [45]. In total, 238 POPC molecules were added to form a lipid bilayer. The rest of the periodic box was filled with water molecules (TIP3P model), 90 potassium ions, and 86 chloride ions to keep the neutrality of the system and provide appropriate ionic strength. Molecular dynamics (MD) simulation was performed in the NAMD 2.13 program [46] with Charmm36 force field [47]. The parameter files for PIP2 were obtained using the ParamChem server employing CGenFF (CHARMM General Force Field) for small molecules [48]. The equilibration and then the production MD simulations were performed at a constant temperature of 298 K and a pressure of 1 bar. The group pressure and the Langevin dynamics were used and the simulation time step was set to 1 fs. Van der Waals and short-range electrostatic interactions with a cutoff 10 Å and 8–10 Å switching function were used. Long-range electrostatic interactions were computed using the Particle Mesh Ewald summation scheme [49]. Each step of the equilibration consisted of energy minimization (10,000 steps) and 20 ns MD simulation with gradual releasing restraints imposed on the system: (i) restrained protein and membrane, (ii) restrained protein, (iii) restrained protein backbone, and (iv) no restraints. Such a procedure was used to obtain stable membrane-protein interactions. The whole system was additionally equilibrated for 200 ns without restraints and the production MD took 500 ns.

The phosphatidic acid (PA) head group docking to the ROMK2 channel and ROMK2-PIP2 complex was performed in the ICM-Pro v.3.8 program (https://www.molsoft.com/icm_pro.html) [50] by "ICM-Docking" method. The docking box was set to include both the primary binding site for PIP2 and the predicted secondary binding site. In ICM-Docking five types of interaction potentials represent the receptor pocket: (i) van der Waals potential for a hydrogen atom probe, (ii) van der Waals potential for a heavy-atom probe (generic carbon of 1.7 Å radius), (iii) optimized electrostatic term, (iv) hydrophobic terms, and (v) a lone-pair-based potential, which reflects directional preferences in hydrogen bonding. The energy terms are based on the all-atom vacuum force field ECEPP/3 with appended terms to account for the solvation free energy and entropic contribution. Conformational sampling is based on the biased probability Monte Carlo (BPMC) procedure [51], which randomly selects a conformation in the internal coordinate space and then makes a step to a new random position independent of the previous one but according to a predefined continuous probability distribution. After each random step, a full local minimization is used to improve the efficiency of the procedure. The ICM-Docking relies on global optimization of the entire flexible ligand in the receptor field and combines large-scale random moves of several types with gradient local minimization and a search history mechanism.

3. Results

3.1. Identification of intracellular neighborhood of ROMK2 channel by proximity biotinylation

The Turbo-ID method was utilized to identify the protein neighborhood of the ROMK2 channel (Fig. 1a). The plasmid carrying the fusion of ROMK2 to TURBO mutant of biotin ligase BirA* was constructed for this purpose [28,52]. Our initial focus was on mitochondrial proteins and we anticipated non-specific biotinylation of proteins due to stochastic

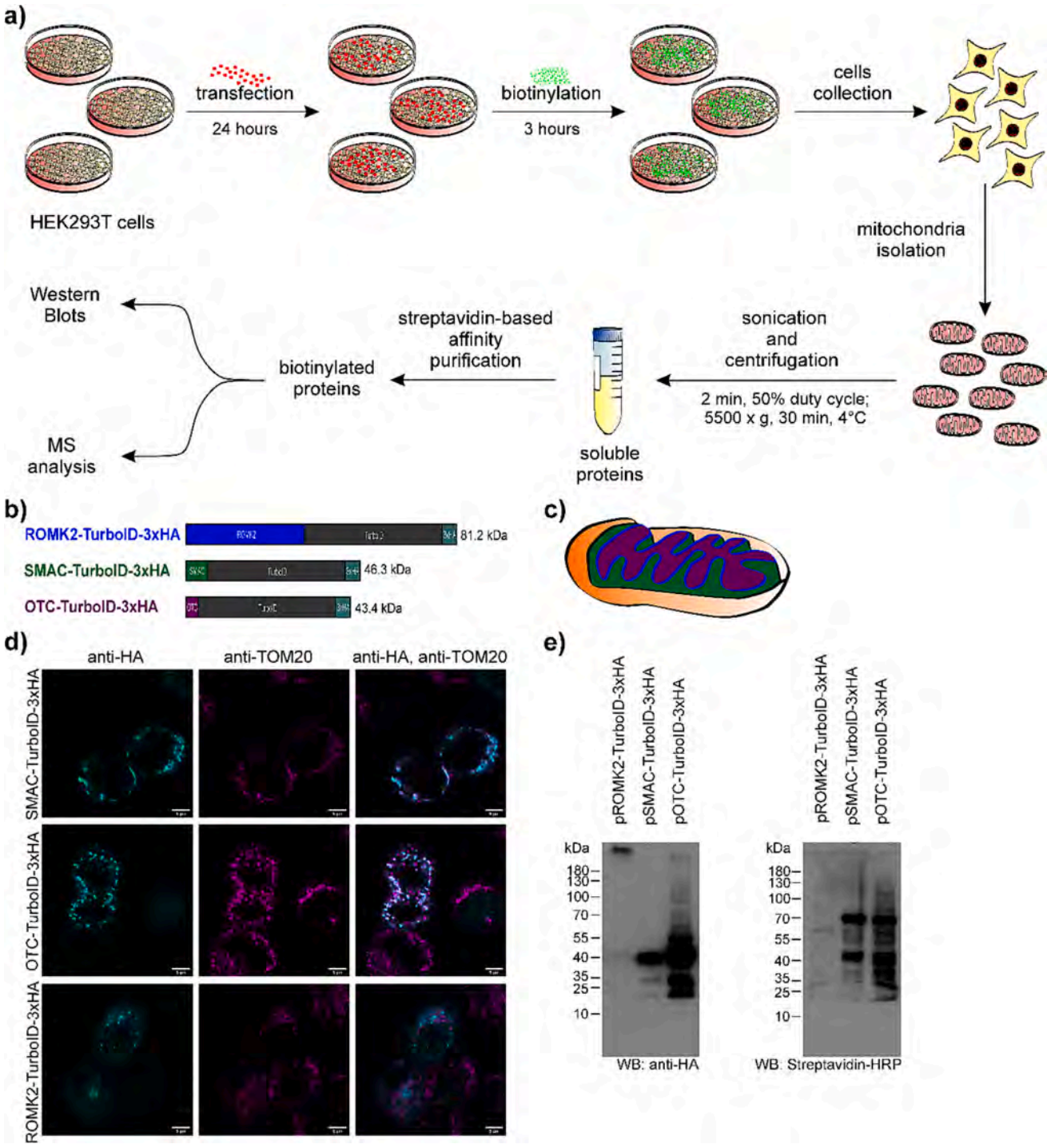

Fig. 1. Detection of the neighborhood of ROMK2 by proximity biotinylation. a A schematic illustration of the TurboID experiment. *From left*: cells were transfected with pcDNA3.1 (negative control), pROMK2-TurboID-3xHA, pSMAC-TurboID-3xHA, and pOTC-TurboID-3xHA plasmids followed by incubation for 3 h with biotin. After harvesting, the mitochondria enriched fraction was isolated and solubilized in the presence of detergent. Insoluble proteins were pelleted by centrifugation. The biotinylated proteins were purified by streptavidin affinity chromatography. The proteins were then analyzed by SDS-PAGE/Western Blot and mass spectrometry. b A schematic representation of the proteins produced by expression constructs used in TurboID experiments: pROMK2-TurboID-3xHA, pSMAC-TurboID-3xHA, and pOTC-TurboID-3xHA. c A schematic visualization of predicted localization of ROMK2-TurboID-3xHA, SMAC-TurboID-3xHA, and OTC-TurboID-3xHA proteins within mitochondria. d A subcellular localization of TurboID fusions. Cells transfected with plasmids producing SMAC-TurboID-3xHA, OTC-TurboID-3xHA, and ROMK2-TurboID-3xHA proteins were incubated with anti-HA (1:200, Sigma Aldrich) and anti-TOM20 (1:500, Sigma Aldrich) antibodies followed by staining with fluorescently labeled secondary antibodies. e An SDS-PAGE/Western Blot analysis of mitochondria-enriched fraction isolated from cells transfected with pROMK2-TurboID-3xHA, pSMAC-TurboID-3xHA, and pOTC-TurboID-3xHA plasmids and incubated with 500 μM biotin. The expression of the TurboID fusions was probed using anti-HA antibody (1:1000, Sigma Aldrich), and the protein biotinylation was detected using streptavidin-HRP (1:40,000 Thermo Fischer Scientific).

diffusion and molecular crowding within both mitochondrial compartments, including the mitochondrial intermembrane space and the matrix. To address this, additional fusions of TurboID-3xHA ligase with OTC (ornithine transcarbamylase) and SMAC (second mitochondria-derived activator of caspase) leaders were constructed (Fig. 1b). The OTC leader directs the localization of the OTC-TurboID-3xHA fusion protein to the mitochondrial matrix [53–55], while the SMAC leader determines the mitochondrial intermembrane space localization of the SMAC-TurboID-3xHA fusion protein [56,57] (Fig. 1c). The endogenous activity of the ROMK2 protein has been described in the rat H9c2 cell line [19,20]. However, despite several attempts, the transfection efficiency of this line was unsatisfactory, both with PEI as well with the H9c2(2–1) Cell Avalanche™ Transfection Reagent (EZBiosystems) (not shown). As a result, all experiments were conducted using HEK293T cells.

To study the subcellular localization of created fusion proteins cells were transfected with pROMK2-TurboID-3xHA, pSMAC-TurboID-3xHA, and pOTC-TurboID-3xHA plasmids, and stained with anti-HA antibody, which specifically recognizes the 3xHA-tag located at the C-terminus of the fusion proteins, as well as with the anti-TOM20 antibody as the mitochondrial marker (Fig. 1d). A close co-localization of the SMAC-TurboID-3xHA and OTC-TurboID-3xHA proteins with TOM20 was observed. However, the ROMK2-TurboID-3xHA protein displayed only partial colocalization with the mitochondrial marker.

In the initial step for TurboID experiments, the conditions of cell transfection with plasmids pROMK2-TurboID-3xHA, pSMAC-TurboID-3xHA, and pOTC-TurboID-3xHA were optimized (Sup. Fig. 4a). Western Blot analysis revealed that all constructs were expressed in HEK293T cells and the most efficient synthesis of the ROMK2-TurboID-3xHA protein was observed when 2.5 μg of DNA and PEI:DNA ratio 4:1 was used. Similarly, the highest production of SMAC-TurboID-3xHA and OTC-TurboID-3xHA was also observed in these conditions (Sup. Fig. 4a).

The optimization of biotinylation conditions was performed on cells transfected with the pROMK2-TurboID-3xHA plasmid (2.5 μg DNA; 4:1 PEI:DNA ratio). Two concentrations of biotin (50 μM and 500 μM) and three biotinylation times (20, 60, and 180 min) were evaluated. The highest level of biotinylation was observed after 180 min, however, there was no significant difference observed in biotinylation levels between the two concentrations of biotin (Sup. Fig. 4b, left panel). Additionally, the biotinylation efficiency at 3-h biotinylation was assessed for the remaining constructs, i.e. pSMAC-TurboID-3xHA and pOTC-TurboID-3xHA. The results indicate a significant increase in the level of biotinylated proteins for pSMAC-TurboID-3xHA with a biotin concentration of 500 μM, compared to 50 μM. In contrast, the opposite trend was observed for pOTC-TurboID-3xHA (Sup. Fig. 4b, right panel).

SDS-PAGE/Western Blot analysis of cells transfected with pROMK2-TurboID-3xHA revealed a signal corresponding to a mass >180 kDa, instead of the expected ROMK2-TurboID-3xHA monomer mass of 81.3 kDa. The native ROMK2 protein is a homotetramer, so the presence of a high mass form may indicate the high stability of the ROMK2 protein oligomers under denaturing conditions. Similar behavior was observed for the ROMK2-6xHis protein overproduced in *E. coli* [41]. Additionally, it was observed that the ROMK2-TurboID-3xHA protein undergoes partial degradation, releasing a protein with a mass of about 40 kDa, which corresponds to the mass of TurboID-3xHA (38.8 kDa). In the case of cells transformed with pSMAC-TurboID-3xHA and pOTC-TurboID-3xHA the production of proteins with a mass of about 40 kDa was observed, which corresponds to the expected masses of corresponding fusion TurboID proteins (46.3 kDa and 43.4 kDa, respectively) (Fig. 1b). Western blot analysis with streptavidin-HRP showed increased level and the number of biotinylated proteins for all constructs in comparison to the controls (Sup. Fig. 4b, Sup. Fig. 5), but the level of biotinylation was much lower for ROMK2-TurboID-3xHA than for SMAC-TurboID-3xHA and OTC-TurboID-3xHA (Fig. 1e).

To investigate the biotinylation of proteins the intracellular fractions enriched with mitochondria from cells transfected with pcDNA3.1 (negative control), pROMK2-TurboID-3xHA, pSMAC-TurboID-3xHA, and pOTC-TurboID-3xHA plasmids and incubated with biotin were isolated (Fig. 1e, Sup. Fig. 6). We opted to use only partially purified mitochondria fractions due to low yield of pure mitochondria preparations. These fractions were found to contain all of the mitochondrial marker succinate dehydrogenase (SDHA) (Sup. Fig. 6a), however, proteins characteristic for other membrane compartments like plasma membrane (Na^+, K^+-ATPase), and ER (TMX1) were also present in these fractions (Sup. Fig. 6b, c). Intracellular fractions enriched with mitochondria contained the majority of SMAC-TurboID-3xHA and OTC-TurboID-3xHA, and ROMK2-TurboID-3xHA (Sup. Fig. 6d) but biotinylation in these fractions was weakest for ROMK2-TurboID-3xHA (Fig. 1e, Sup. Fig. 6e).

A series of TurboID experiments were performed (Fig. 1a) in which cells were transfected and biotinylated under optimized conditions. Biotinylated proteins retained on the streptavidin beads were analyzed by Western Blot (Sup. Fig. 5) and identified by mass spectrometry.

By comparing the frequency of occurrence of particular proteins and the number of identified peptides in the pROMK2-TurboID-3xHA sample against controls (pcDNA3.1, pOTC-TurboID-3xHA, and pSMAC-TurboID-3xHA), it was possible to identify proteins specific for the ROMK2-TurboID-3xHA proxisome. The focus was on proteins that were uniquely detected in at least three out of seven experiments. Based on this criterion 45 proteins were identified as potential proteins that could be in proximity and interact with the ROMK2 protein (Table 1).

Identified proteins were classified according to subcellular localization (Fig. 2a, left panel). Of the 45 proteins, 26.6 % were identified as nuclear, 23.9 % as cytoplasmic, 12.8 % as proteins located in the plasma membrane, 12.8 % located in the vesicles, and 9.2 % in the endoplasmic reticulum. Only 3.7 % of the analyzed proteins were assigned a mitochondrial localization. The identified proteins, based on the annotation of three different databases (UniProt (www.uniprot.org), Human Protein Atlas (www.proteinatlas.org), MitoCarta3.0 (http://www.broadinstitute.org/mitocarta)), were also classified according to their functions in different biological processes (Fig. 2a, right panel). It was determined that 19.7 % of the identified proteins are involved in the DNA or RNA metabolism, 16.7 % are scaffold proteins associated with cellular transport and the same amount of proteins perform signaling functions. 13.6 % of the identified proteins are involved in the transcription and translation processes. On the other hand, 10.6 % of the identified proteins are related to transport across biological membranes. Among the ROMK2-TurboID-3xHA potential proxisome, some proteins play roles in metabolism (6.1 %), apoptosis (6.1 %), development and differentiation (6.1 %), and phosphorylation (4.5 %).

Functional protein association networks between identified proteins were visualized using the Cytoscape program (cytoscape.org) (Fig. 2b). The networks include different tubulins (Fig. 2b i), as well as clathrin and other proteins involved in clathrin-dependent endocytosis (Fig. 2b ii). Additionally, four signal recognition particle (SPR) proteins involved in the co-translational transport of proteins to the ER were identified (Fig. 2b iii), as well as chaperones from the DnaJ family (DnaJC16, DnaJC11, DnaJA1, DnaJA3) implicated in folding and/or transport of proteins into the ER or mitochondria (Fig. 2b iv). Mitochondrial localization of ROMK2 was further supported by the identification of subunits of TOM and TIM complexes, which translocate proteins across the outer and inner mitochondrial membranes, respectively (Fig. 2b v). Specifically, the TOM40, TIM44, and TIM50 proteins were detected in ROMK2-TurboID-3xHA samples. In addition to TIM44 and TIM50 other proteins i.e. TIM16 and TIM21, that together form the TIM23 complex located in the inner mitochondrial membrane, were identified in the SMAC-TurboID-3xHA and OTC-TurboID-3xHA samples (Sup. Table 1). The presence of mitochondrial acylglycerol kinase (AGK), on the other hand, was detected only in the ROMK2-TurboID-3xHA samples. AGK is a bifunctional protein that constitutes a subunit of the TIM22 complex involved in the insertion of polytopic membrane proteins into the IMM but also plays a role in lipid metabolism by phosphorylating

Table 1
Unique proteins identified in ROMK2-TurboID-3xHA samples by mass spectrometry. The columns list the protein name, gene, predicted protein mass, the number of counts in individual experiments ("score"), the number of identified peptides in individual experiments, and the predicted localization of the protein. The localization was determined based on the annotations from Uniprot (U) (www.uniprot.org) and the Human Protein Atlas (A) (www.proteinatlas.org) databases and is indicated as CS (cytoskeleton), C (cytoplasm), GA (Golgi apparatus), N (nucleus), ER (endoplasmic reticulum), PM (plasma membrane), V (vesicle), and M (mitochondria). The score and the number of identified peptides in individual experiments were marked when the protein was also detected in other samples, i.e. c - control (pcDNA3.1), o - OTC-TurboID-3xHA, s - SMAC-TurboID-3xHA. Proteins are arranged in decreasing order of the sum of the scores.

Protein	Gene	Mass [Da]	Score							Peptides							Localization
			Exp. 1	*Exp. 2*	*Exp. 3*	*Exp.4*	*Exp. 5*	*Exp. 6*	*Exp. 7*	*Exp. 1*	*Exp. 2*	*Exp. 3*	*Exp.4*	*Exp. 5*	*Exp. 6*	*Exp. 7*	
Tubulin beta chain	**TUBB**	50,007	462	237	292	0	$1002^{c219,\ o288}$	834^{o194}	145^{c66}	10	5	5	0	$14^{c6,\ o6}$	13^{o6}	3^{c1}	$CS^{U,\ A}$
Zinc finger CCCH-type antiviral protein 1	**ZC3HAV1**	102,793	115^{o51}	54	99	113	204^{s71}	$260^{o96,\ s233}$	68	3^{o1}	1	1	1	5^{s1}	$7^{o1,\ s4}$	2	$C^{U,\ A}/GA^{A}/N^{U}$
Extended synaptotagmin-1	**ESYT1**	123,194	112	75	127	0	$124^{o64,\ s52}$	198^{s84}	132^{s77}	2	1	2	0	$2^{o1,\ s1}$	4^{s1}	2^{s1}	$ER^{U,\ A}/PM^{U,\ A}$
G patch domain-containing protein 8	**GPATCH8**	164,834	194	60	51	0	$128^{c125,\ s39}$	$193^{c131,\ o97,\ s59}$	$95^{c66,\ o61,\ s60}$	2	1	1	0	$3^{c3,\ s1}$	$4^{c2,\ o2,\ s1}$	$1^{c1,\ o1,\ s1}$	M^{A}/N^{A}
Phosphatidylinositol-binding clathrin assembly protein	**PICALM**	70,848	164^{o45}	0	58	0	126	248^{s159}	95	4^{o1}	0	1	0	2	4^{s3}	2	$GA^{U}/\ N^{U}/PM^{U}/\ V^{A}$
Plakophilin-4	**PKP4**	142,431	137	0	75	0	35	215^{o121}	219^{o44}	2	0	1	0	1	8^{o2}	4^{o1}	CS^{U}/PM^{U}
DnaJ homolog subfamily C member 16	**DNAJC16**	90,948	42	47	0	0	197	232	77	1	1	0	0	4	5	2	$C^{U,\ A}/V^{A}$
Unconventional myosin-VI	**MYO6**	150,700	96	0	50	0	102	212^{s104}	131	1	0	1	0	1	3^{s3}	2	$C^{U}\ /GA^{U}\ /N^{U,\ A}/\ PM^{U}$
Polyadenylate-binding protein 1	**PABPC1**	70,810	61	48	51	0	200	185^{s34}	0	2	1	1	0	5	5^{s1}	0	$C^{U,\ A}/N^{U}$
Acylglycerol kinase	**AGK**	47,475	144	108	127	0	0	139	0	1	1	1	0	0	1	0	$M^{U,\ A,\ M}/V^{A}$
Inosine-5′-monophosphate dehydrogenase 2	**IMPDH2**	56,138	47	0	0	70	253	119	0	1	0	0	1	5	1	0	$C^{U,\ A}/N^{U}$
Fibronectin type-III domain-containing protein 3A	**FNDC3A**	133,377	49	99^{s63}	110^{s81}	0	0	70	103	1	1^{s1}	1^{s1}	0	0	1	1	$C^{A}/GA^{U,\ A}\ /N^{A}/\ V^{A}$
60S ribosomal protein L6	**RPL6**	32,754	40	0	50	46	$116^{s38,\ o81}$	$52^{o72,\ s45}$	$123^{c140,\ o91,\ s99}$	1	0	1	1	$4^{s1,\ o2}$	$1^{o1,\ s1}$	$2^{c2,\ o1,\ s1}$	$C^{U}/CS^{A}/ER^{U}$
Nucleolar protein 56	**NOP56**	66,331	0	59	69	0	$187^{c56,\ 0136}$	74	0	0	1	1	0	$3^{c1,\ o3}$	1	0	$C^{U}/N^{U,\ A}$
RNA-binding protein 39	**RBM39**	59,573	43	0	0	0	153	76^{s41}	75	1	0	0	0	3	1^{s1}	1	$CS^{A}/N^{U,\ A}$
Erbin	**ERBIN**	158,798	85	0	0	0	0	112	133	2	0	0	0	0	5	4	$N^{U,\ A}/PM^{U,\ A}$
Neurogenic locus notch homolog protein 1	**NOTCH1**	283,636	59	0	0	0	55	105	92	1	0	0	0	1	5	3	$N^{U,\ A}/PM^{U,\ A}$
60S ribosomal protein L7	**RPL7**	29,253	140	0	0	54	60^{o48}	45	0	3	0	0	1	2^{o1}	1	0	$C^{U,\ A}/ER^{A}/N^{U,\ A}$
Kinase D-interacting substrate of 220 kDa	**KIDINS220**	197,707	57	0	0	0	69	97^{o31}	72	1	0	0	0	1	2^{o1}	1	$V^{U,\ A}$
Pre-mRNA-processing factor 40 homolog A	**PRPF40A**	108,967	0	0	54	0	141	100	0	0	0	1	0	3	2	0	$N^{U,\ A}$
Vesicle-associated membrane protein-associated protein A	**VAPA**	28,059	106^{o48}	49	40	0	41	58^{s61}	0	2^{o1}	1	1	0	1	2^{s2}	0	$ER^{U,\ A}/N^{A}/PM^{U}$
Unconventional myosin-Id	**MYO1D**	116,772	119	0	0	0	94	70	0	2	0	0	0	1	1	0	$C^{U,\ A}/V^{U}$
Protein numb homolog	**NUMB**	71,311	38	0	0	0	62	107	72	1	0	0	0	1	3	2	PM^{U}/V^{U}
Clathrin heavy chain 1	**CLTC**	192,918	48	0	66	0	82	82	0	1	0	1	0	2	1	0	$C^{U,\ A}/V^{A}$
Copper-transporting ATPase 2	**ATP7B**	158,496	67	0	0	0	0	115	88	1	0	0	0	0	3	1	$C^{U}/GA^{U,\ A}/M^{U}/\ V^{U}$
40S ribosomal protein S16	**RPS16**	16,527	59	0	84	0	64^{c72}	52	0	1	0	1	0	1^{c1}	1	0	$C^{U,\ A}/ER^{A}/N^{U}$
Prosaposin	**PSAP**	59,545	60	50	91	0	0	0	$57^{c89,\ o48,\ s50}$	1	1	2	0	0	0	$1^{c1,\ o1,\ s1}$	$V^{U,\ A}$
60S ribosomal protein L18	**RPL18**	20,979	0	62	0	0	118	77	0	0	1	0	0	2	1	0	$C^{U,\ A}/ER^{U,\ A}/N^{A}$
40S ribosomal protein S3	**RPS3**	45,382	0	0	0	52	122	70	0	0	0	0	1	3	2	0	$C^{U,\ A}/C^{U}/ER^{A}\ /M^{U}/\ N^{A}$
Numb-like protein	**NUMBL**	65,449	0	0	0	0	52	118	71	0	0	0	0	2	3	2	C^{U}

(*continued on next page*)

Table 1 (*continued*)

Protein	Gene	Mass [Da]	Score							Peptides							Localization
			Exp. 1	*Exp. 2*	*Exp. 3*	*Exp.4*	*Exp. 5*	*Exp. 6*	*Exp. 7*	*Exp. 1*	*Exp. 2*	*Exp. 3*	*Exp.4*	*Exp. 5*	*Exp. 6*	*Exp. 7*	
60S ribosomal protein L11	**RPL11**	20,424	52	0	52	46	90	0	0	1	0	1	1	3	0	0	$C^{U}/N^{U}/V^{A}$
Vezatin	**VEZT**	89,299	0	0	0	0	33	103	102	0	0	0	0	1	1	1	$C^{A}/N^{U, A}/PM^{U}$
Putative tRNA (cytidine(32)/guanosine(34)-2′-O)-methyltransferase	**FTSJ1**	36,562	45	0	0	0	34	83^{s39}	70	1	0	0	0	1	2^{s1}	1	$C^{U, A}$
Leucine-rich repeat-containing protein 59	**LRRC59**	35,231	57	0	57	0	52	65^{s34}	0	1	0	1	0	1	1^{o4}	0	$ER^{U, A}/N^{U}$
Diacylglycerol kinase epsilon	**DGKE**	65,173	60	0	0	0	0	83	84	1	0	0	0	0	2	1	$C^{U, A}/N^{A}/PM^{U, A}$
Cellular tumor antigen p53	**TP53**	44,085	42	0	49	0	57	77	0	1	0	1	0	2	1	0	$C^{U, A}/CS^{U}/N^{U, A}/V^{U}$
Epsin-3	**EPN3**	68,318	54	0	0	0	48	49	61	1	0	0	0	1	1	1	$C^{U}/N^{U, A}/V^{A}$
Guanine nucleotide-binding protein G(s) subunit alpha isoforms XLas	**GNAS**	111,553	63	0	0	0	85	50	0	1	0	0	0	1	1	0	$C^{A}/N^{A}/PM^{U, A}$
60S ribosomal protein L8	**RPL8**	28,191	0	0	47	0	91	57	0	0	0	1	0	2	1	0	$C^{U, A}/ER^{A}/N^{A}$
Kinesin-like protein KIF14	**KIF14**	187,479	97	0	59	0	0	34	0	3	0	1	0	0	1	0	$C^{U, A}/CS^{U}/N^{U}$
Sodium-dependent neutral amino acid transporter B(0)AT2	**SLC6A15**	82,518	0	0	0	0	65	68	48	0	0	0	0	2	1	1	$N^{A}/PM^{U}/V^{A}$
ER membrane protein complex subunit 8	**EMC8**	24,126	38	0	0	0	0	73	67	1	0	0	0	0	3	1	C^{A}/ER^{U}
CCR4-NOT transcription complex subunit 1	**CNOT1**	268,653	54	0	0	0	52	67	0	1	0	0	0	1	2	0	C^{A}/N^{U}
Nuclear ubiquitous casein and cyclin-dependent kinase substrate 1	**NUCKS1**	27,280	0	54	51	0	39	0	0	0	1	1	0	1	0	0	$N^{U, A}$

monoacylglycerol (MAG) and diacylglycerol (DAG) to lysophosphatidic acid (LPA) and phosphatidic acid (PA), respectively [31]. Curiously, another enzyme that carries out an analogous reaction in ER and PM, diacylglycerol kinase ε (DGKE) was also among the proteins of the unique proxisome of ROMK2.

Several other proteins of the proxisome of ROMK2-TuboID-3xHA also turned our attention including PARP1 [58] and p53 proteins, which are translocated into the mitochondria in response to oxidative stress [59,60]. Linkage analysis between proteins shows a relationship between the apoptotic p53 protein and peroxiredoxin 1 (PRDX1) [60,61], which was also identified in the ROMK2-TurboID-3xHA samples. In addition, among potential ROMK2 neighbors was also inosine-5′-monophosphate dehydrogenase 2 (IMPDH2) [62,63]. IMPDH catalyzes the NAD-dependent oxidation of inosine monophosphate (IMP) to xanthosine 5′-monophosphate (XMP), which is an intermediate metabolite in the production of guanosine triphosphate (GTP). On the other hand, IMP can be converted to ATP [62]. Therefore, IMPDH regulates not only the production of GTP but also the amount of produced ATP. Additionally, among the identified proteins, was the elusive protein GPATCH8 with potential mitochondrial localization [64]. In summary, the analysis of proximal proteins revealed that the ROMK2 variant is distributed across multiple membrane compartments, including vesicles, the endoplasmic reticulum, and mitochondria.

3.2. *ROMK2 channel physically interacts with AGK and DGKE lipid kinases*

Identification of proteins adjacent to the ROMK2 may suggest their physical interactions with the channel. To verify this possibility co-immunoprecipitation (Co-IP) between ROMK2 and selected proteins i.e. AGK, DGKE, PARP1, p53, PRDX1, IMPDH2, and GPATCH8 was performed. For these studies, plasmids producing these proteins with the FLAG tag at their C-ends were co-transformed with the plasmid producing the ROMK2 tagged with V5 epitope at its C-terminus (pROMK2-V5). As controls cells were transfected only with the pROMK2-V5 plasmid or only with the plasmid producing a potential interaction partner. Proteins were immunoprecipitated with anti-V5 or anti-FLAG magnetic beads. Immunoprecipitated fractions were analyzed by PAGE/Western Blot (Fig. 3, Fig. 4, and Sup. Fig. 7). Probing with the anti-KCNJ1 antibody revealed the presence of the ROMK2 protein only in the control samples from cells transfected with the pROMK2-V5 plasmid precipitated with the anti-V5 antibody, but not with anti-FLAG antibody (Fig. 3a, left panel; Fig. 4a and b). In these samples, bands corresponding to different forms of the ROMK2-V5 protein were observed: monomer (c.a. 40 kDa), dimer (70–100 kDa), as well as higher oligomeric forms (>130 kDa) (e.g. Fig. 3a, left panel). No signal was observed when the anti-FLAG, anti-AGK, or anti-DGKE antibody was used (Fig. 3b and c, left panels; Fig. 4a, right panel) demonstrating the specificity of these antibodies.

Proteins were also precipitated by the anti-FLAG antibody from lysates of cells transfected with either a plasmid producing a potential interaction partner or co-transfected with a plasmid producing a potential interaction partner and pROMK2-V5 plasmid. After SDS-PAGE/Western Blot analysis of immunoprecipitation products with the anti-FLAG antibody (Fig. 3b and Sup. Fig. 7), anti-AGK antibody (Fig. 3c), or the anti-DGKE antibody (Fig. 4a), it was found that all potential partner proteins were retained on the anti-FLAG antibody resin. Bands corresponding to the masses of these proteins were observed, both in the samples of cell lysates transfected with the plasmid producing the potential partner as well as co-transfected with the pROMK2-V5 plasmid. On the other hand, immunoblotting with the anti-KCNJ1 antibody revealed a signal corresponding to the ROMK2 protein only in the samples from lysates of cells co-transfected with the pROMK2-V5 and pAGK-FLAG plasmids (Fig. 3, and Sup. Fig. 7), as well as pROMK2-V5 and pDGKE-FLAG plasmids (Fig. 4) demonstrating that the ROMK2-V5 protein co-precipitates specifically with AGK-FLAG and DGKE-FLAG

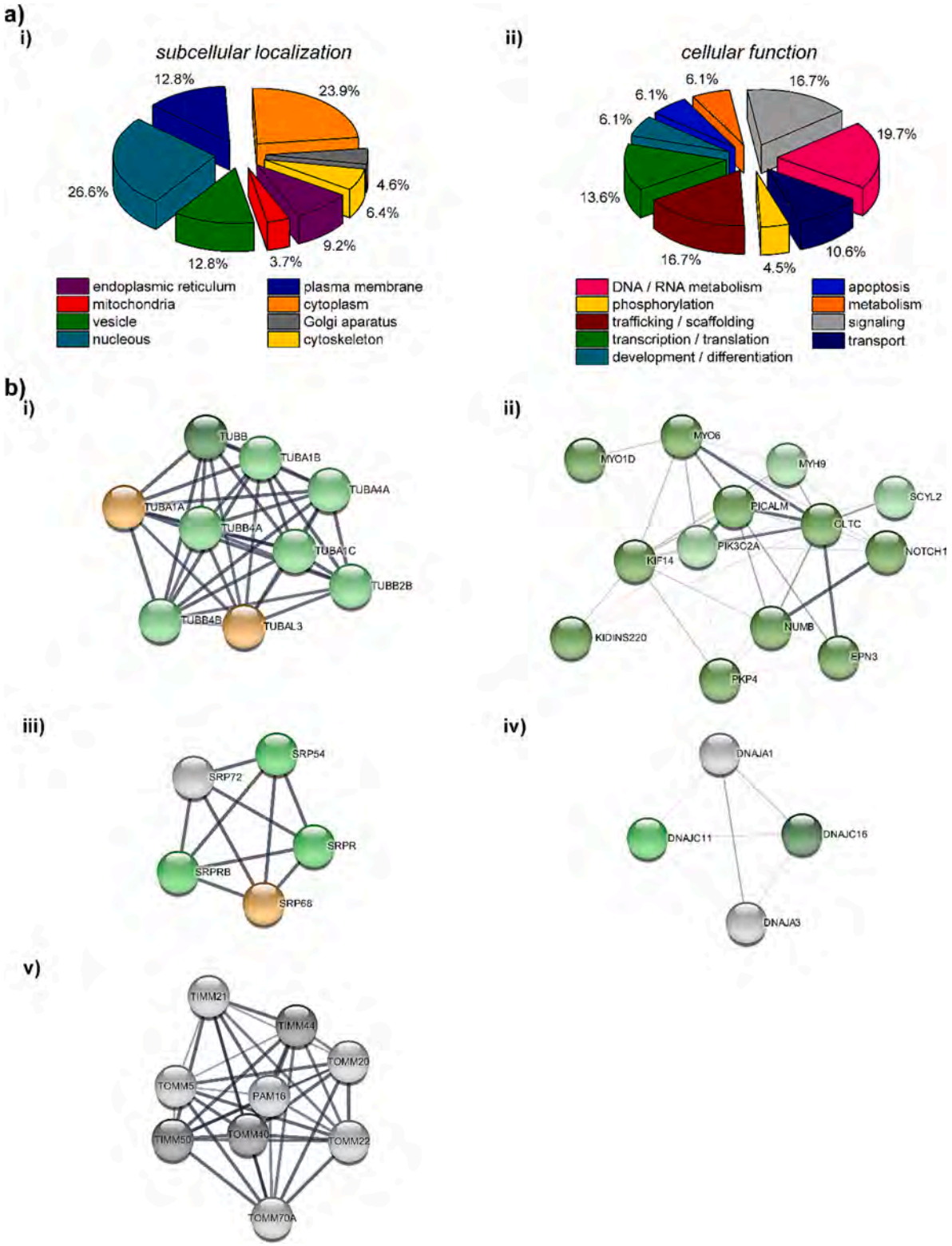

Fig. 2. Characterization of ROMK2 proxisome. a Classification of the identified proteins by (i) subcellular localization and (ii) cellular function. The proteins were characterized based on the information in UniProt (www.uniprot.org) and Human Protein Atlas (www.proteinatlas.org) databases. b Functional association networks among proteins of the proxisome. Clustering of functional groups was performed using protein-protein interactions from the STRING databases. The figure shows the relationship between: i) tubulins, ii) proteins involved in clathrin-dependent endocytosis and vesicular transport, iii) signal recognition particle (SPR) proteins involved in the co-translational transport of proteins into the ER, iv) DnaJ family chaperones involved in the folding/import of proteins and organization of membranes of ER and mitochondria, v) translocases of mitochondrial outer and inner membranes. The nodes represent proteins, which are colour-coded according to the frequency of protein identification in the ROMK2-TurboID-3xHA proxisome: dark green nodes - proteins identified as unique at least three times, light green nodes - proteins identified as unique less than three times, orange nodes - proteins identified as unique only after oxidative stress (treatment cells with H_2O_2 or t-BHP), gray nodes - proteins also found in SMAC-TurboID-3xHA and OTC-TurboID-3xHA controls. The thickness of the lines between nodes reflects the likelihood of interactions between proteins.

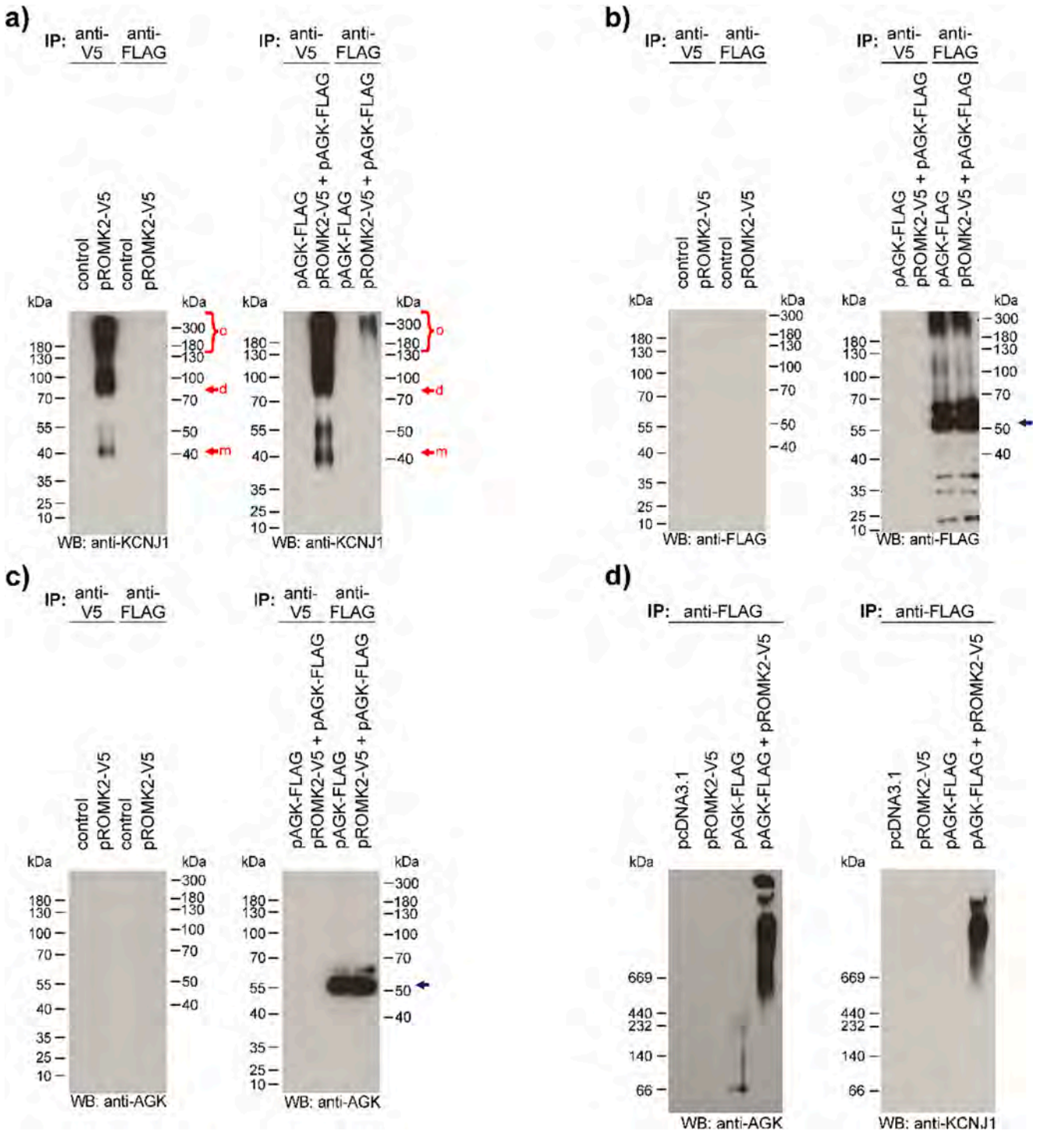

Fig. 3. Detection of ROMK2-AGK complexes. a-c SDS-PAGE/Western blot analysis of samples from Co-IP experiments. Cell lysates from control cells and cells transfected with pROMK2-V5 or/and pAGK-FLAG were subjected to Co-IP with anti-V5 and anti-FLAG antibodies. Proteins were detected (WB) using the following antibodies: a anti-KCNJ1 (1:200, Sigma Aldrich), red arrows indicate predicted positions of monomers (m), dimers (d), and oligomers (o) of ROMK2-V5, b anti-FLAG (1:1000; Origene), and c anti-AGK (1:500, Origene), blue arrows indicate the predicted position of AGK. d Blue Native-PAGE/Western blot analysis of samples from Co-IP samples. Samples from cells transfected with the indicated plasmids after immunoprecipitation with anti-FLAG antibody, separated by Blue Native-PAGE (4–13 %) and detected with anti-AGK (1:1000; Origene), and anti-KCNJ1 (1: 200, Sigma Aldrich) antibodies.

proteins. Since AGK is a dual-function protein we wondered whether its complex with ROMK2 channel contains also another component of TIM22 translocase i.e. TIM29. However, our analysis revealed that this was not the case (Sup. Fig. 8).

3.3. Complexes of ROMK2 channel with AGK and DGKE are captured in native nanodiscs

To further substantiate interactions of ROMK2 with AGK and DGKE lipid kinases, and exclude the influence of the solubilization conditions on the obtained results, amphipathic copolymers DIBMA and SMA were

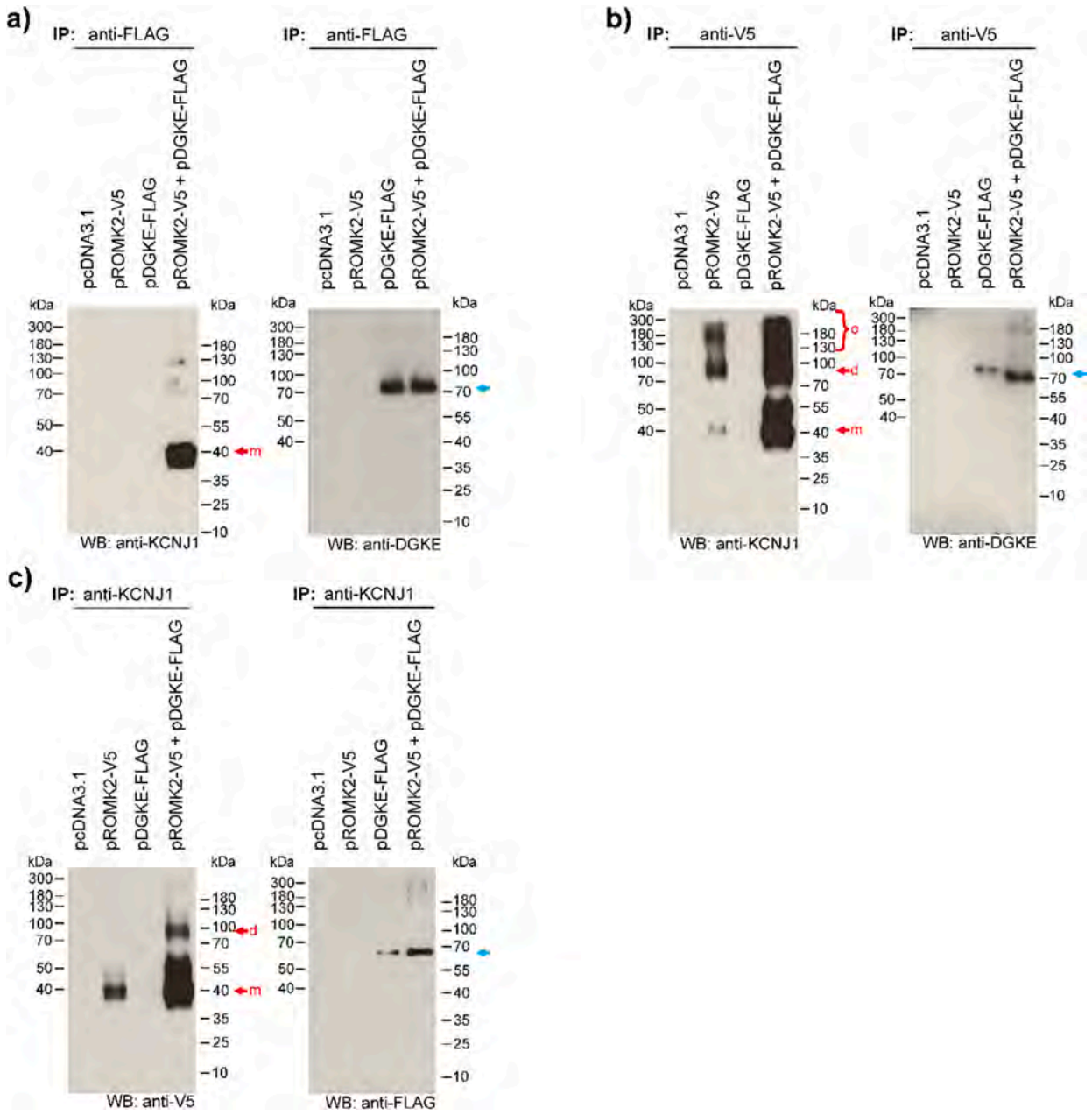

Fig. 4. Interaction of ROMK2 channel with DGKE. SDS-PAGE/Western Blot analysis of Co-IP samples. Immunoprecipitation (IP) was performed using lysates of control cells (pcDNA3.1) and cells transfected with plasmids pROMK2-V5 or pDGKE-FLAG, and cells cotransfected with both plasmids. For immunoprecipitation (IP) following antibodies were used: a anti-FLAG, b anti-V5, c anti-KCNJ1 antibodies. Proteins were detected (WB) with anti-KCNJ1 (1:200, Sigma Aldrich), anti-FLAG (1:1000; Origene), anti-V5 (1:1000, Sigma-Aldrich), and anti-DGKE (1:500, Proteintech) antibodies. Red arrows indicate the predicted positions of monomers (m), dimers (d), and oligomers (o) of ROMK2-V5; light blue arrows indicate the predicted position of DGKE.

used (Fig. 5a). These copolymers solubilize membrane proteins along with surrounding lipids to form so-called native nanodiscs, a method previously demonstrated to be effective in isolating and stabilizing membrane protein complexes [65–71]. To test the ability of these co-polymers to solubilize the ROMK2 channel, the mitochondria-enriched fraction isolated from cells transfected with the pROMK2-V5 plasmid was mixed with DIBMA and SMA polymers of different stoichiometries (SMA 1.2:1, SMA 2.3:1, and SMA 3:1). Of the tested polymers, only two DIBMA and SMA 1.2:1 were found to effectively solubilize the ROMK2-V5 protein (Sup. Fig. 9). The solubilization with DIBMA was more efficient than with SMA 1.2:1, and as such, DIBMA was used to solubilize cells co-transfected with pROMK2-V5 and either pAGK-FLAG or pDGKE-FLAG (Fig. 5).

SDS-PAGE/Western Blot analysis showed that both the ROMK2-V5 protein (> 300 kDa) (Fig. 5b left panel) and AGK-FLAG (55 kDa) (Fig. 5b right panel) were solubilized with DIBMA copolymer. As in the previous experiments, also in this case affinity chromatography with anti-V5 and anti-FLAG antibodies was used for protein co-precipitation. A very small amount of the ROMK2-V5 protein was present in the fraction purified against the anti-V5 antibody (Fig. 5b left panel, Co-IP: anti-V5). AGK-FLAG protein was not detected in this sample (Fig. 5b right panel, Co-IP: anti-V5). Further purification of this sample against anti-FLAG antibody and Western Blot analysis of these samples did not reveal the presence of any of the proteins (Fig. 5b, anti-V5/anti-FLAG). In parallel, the same sample was purified against the anti-FLAG antibody (Fig. 5b, Co-IP: anti-FLAG). In this case, Western Blot analysis of the elution fraction showed the presence of both AGK-FLAG (Fig. 5b right panel, Co-IP: anti-FLAG) and ROMK2-V5 proteins (Fig. 5b left panel, Co-

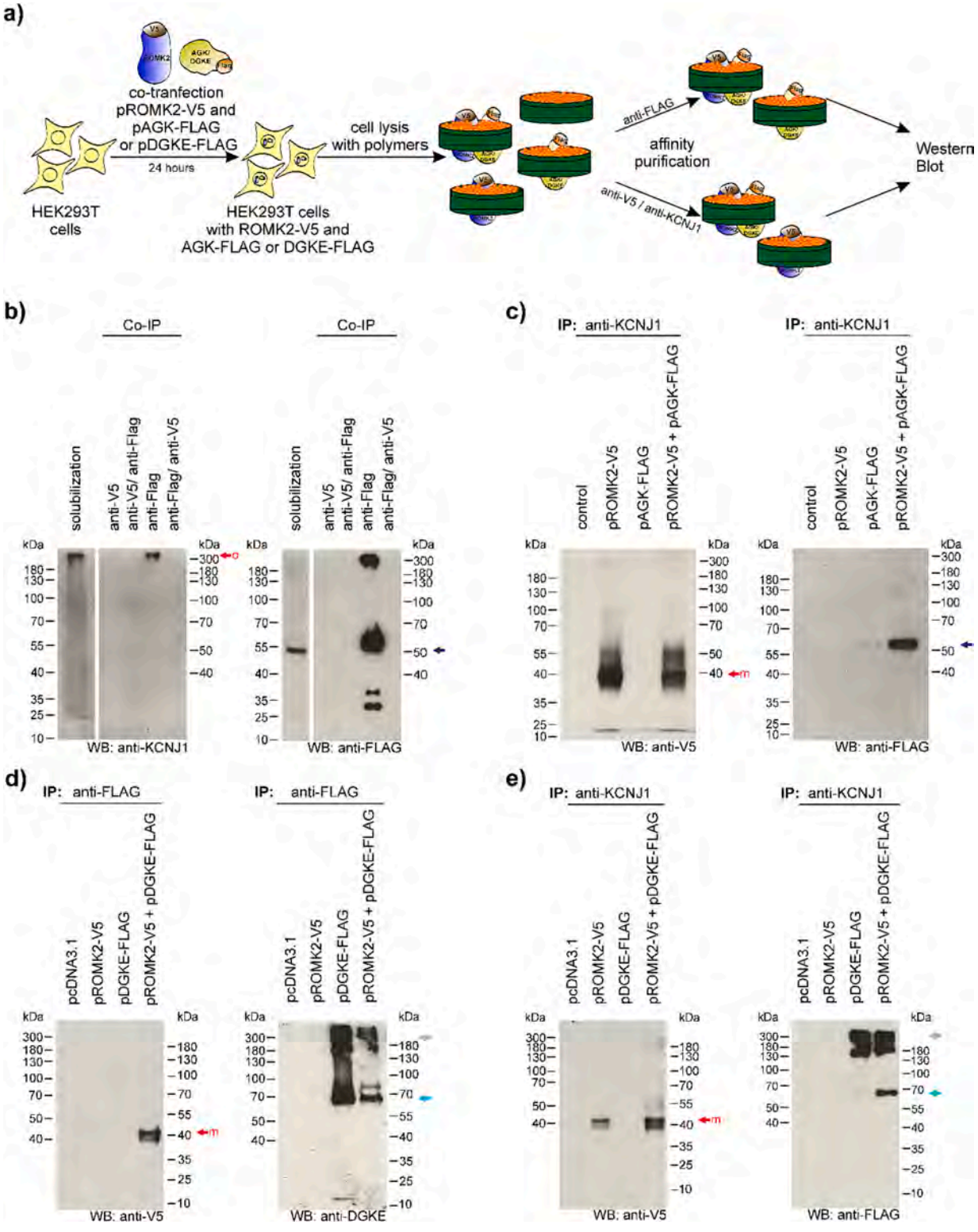

(caption on next page)

Fig. 5. Complexes of ROMK2 and AGK or DGKE are captured in native nanodiscs. a Schematic representation of the Co-IP experiment using polymer nanodiscs. *From left*: Cells were co-transfected with pROMK2-V5 and pAGK-FLAG or pDGKE-FLAG plasmid, then harvested and solubilized in the presence of SMA or DIBMA co-polymers. Samples were centrifuged and soluble proteins were immunoprecipitated with anti-V5, anti-FLAG, or anti-KCNJ1 antibodies. b SDS-PAGE/Western Blot analysis of the Co-IP experiment between ROMK2-V5 and AGK-FLAG proteins solubilized in DIBMA nanodiscs. The first stage of the experiment was performed using anti-V5 or anti-FLAG antibody, followed by the second stage using a second antibody which was an anti-FLAG antibody for the sample first purified against an anti-V5 antibody, and vice versa. ROMK2-V5 protein was detected with the anti-KCNJ1 antibody (1:200, Sigma Aldrich), while AGK-FLAG protein was detected with the anti-FLAG antibody (1:1000; Origene). c Western Blot analysis of the Co-IP experiment between ROMK2-V5 and AGK-FLAG proteins solubilized in DIBMA nanodiscs precipitated with anti-KCNJ1 antibody. ROMK2-V5 protein was detected with anti-V5 antibody (1:1000, Sigma-Aldrich), while AGK-FLAG protein was detected with anti-FLAG antibody (1:1000; Origene). d Western Blot analysis of Co-IP experiment between ROMK2-V5 and DGKE-FLAG solubilized with DIBMA copolymer. Immunoprecipitation (IP) was performed with the anti-FLAG antibody. Detection of proteins with anti-V5 (1:1000, Sigma-Aldrich) – ROMK2-V5 protein, and anti-DGKE (1:500, Proteintech) antibodies. e Western Blot analysis of Co-IP experiment between ROMK2-V5 and DGKE-FLAG proteins against anti-KCNJ1 antibody. Proteins were detected using anti-V5 (1:1000, Sigma-Aldrich), and anti-FLAG antibody (1:1000; Origene) antibodies. Predicted positions of monomers (m), and oligomers (o) of ROMK2-V5 are indicated by red arrows. Blue arrows indicate the predicted position of AGK-FLAG, light blue arrows indicate the predicted position of DGKE-FLAG, and gray arrows indicate positions of bands of unknown origin.

IP: anti-FLAG). Interestingly, the AGK-FLAG protein migrated in the gel not only at 55 kDa as predicted by its molecular weight but also as a form above 300 kDa (Fig. 5b, right panel, Co-IP: anti-FLAG) suggesting the stability of ROMK2-V5/AGK-FLAG complex solubilized in nanodiscs. This sample was purified against the V5- antibody, however, neither ROMK2-V5 nor AGK-FLAG proteins were detected in this case (Fig. 5b, Co-IP: anti-FLAG/anti-V5). This suggests that in the complex with AGK the V5 epitope on ROMK2 is unavailable for the anti-V5 antibody.

Therefore, this experiment was also performed with the immobilized anti-KCNJ antibody raised against a peptide encompassing amino acids 284–368 of ROMK2. When immunoprecipitated samples from cells transfected with pROMK2-V5 as well as from cells cotransfected with pROMK2-V5 and pAGK-FLAG, were probed with anti-V5 antibody the main band of about 40 kDa, corresponding to the monomer of ROMK2-V5 was observed (Fig. 5c left panel). This confirmed the ability of the immobilized anti-KCNJ1 antibody to bind ROMK2-V5 protein. When the anti-KCNJ1 immunoprecipitated sample from cells cotransfected with pROMK2-V5 and pAGK-FLAG was probed with anti-FLAG antibody a specific band of around 55 kDa was observed which confirmed the presence of AGK-FLAG protein (Fig. 5c, right panel) and further substantiated the presence of a protein complex containing ROMK2-V5 and AGK-FLAG.

Affinity chromatography with anti-FLAG and anti-KCNJ1 antibodies was also used for the analogous co-precipitation of native nanodiscs derived from cells co-transfected with pROMK2-V5 and pDGKE-FLAG plasmids. Western Blot analysis of the elution fractions showed the presence of both DGKE-FLAG and ROMK2-V5 proteins (Fig. 5d-e). Thus, the results of the CoIP experiments with native nanodiscs support the physical interaction of ROMK2 with AGK and DGKE proteins.

3.4. ROMK2 channel colocalization with AGK and DGKE

TurboID experiments and immunofluorescence of ROMK2-TurboID-3xHA protein suggested the localization of the ROMK2 protein in various membrane compartments with only a fraction of it in the mitochondria (Fig. 1d). To exclude the influence of the C-terminal TurboID-3xHA on the subcellular localization of the ROMK2 protein the localization of the ROMK2-V5 protein was checked. Similar to the fusion with TurboID-3xHA, this version of ROMK2 only marginally co-localized with the mitochondrial markers: coxIV and the mitochondrial-specific fluorescent dye Mito Red (Fig. 6a). A similar extent of colocalization of ROMK2 with mitochondrial kinase AGK was observed (Fig. 6a). In contrast, strong colocalization was observed between ROMK2-V5 and DGKE (Fig. 6b, c). To get more insight into the membrane compartments where these proteins are located, additional immunostaining was performed with antibodies against calnexin (an ER marker) or EEA1 - an early endosome marker). Triple staining revealed a strong co-localization of ROMK2 and DGKE with the ER marker (Fig. 6b) but only weak colocalization with the early endosome marker (Fig. 6c).

3.5. The effect of enzymatic products of AGK and DGKE on the activity of the ROMK2-6xHis channel

The results of the TurboID and Co-IP experiments suggest a direct physical interaction between the ROMK2 and AGK or DGKE. The AGK performs the phosphorylation reaction of monoacylglycerol (MAG) to lysophosphatidic acid (LPA) or diacylglycerol (DAG) to phosphatidic acid (PA), while DGKE phosphorylates DAG to PA. Therefore, it was checked whether the products of enzymatic activity of these kinases, i.e. LPA and PA, affect the activity of the ROMK2 channel. To accomplish this, a planar lipid bilayer (PLB) system was employed, incorporating ROMK-6xHis protein into a lipid bilayer from native nanodiscs as was shown earlier [41].

Initially, the impact of known modulators on ROMK2 channel activity was confirmed to validate the molecular origin of the observed channel activity. The results showed that ATP/Mg^{2+}, the known inhibitor of mitoK_{ATP} channel [72,73] and ROMK [20,41,74], reduced the probability of opening ROMK2-6xHis channels from 0.98 ± 0.53 to 0.38 ± 0.36 ($n = 16$) (Fig. 7a). Moreover, VU591, the most specific synthetic small molecule blocker of the activity of ROMK channels [75,76], decreased the probability of channel openings from 1.14 ± 0.67 to 0.07 ± 0.08 ($n = 6$) (Fig. 7b). Next, the effect of LPA and PA on ROMK2-6xHis channel activity was tested. Fig. 7c illustrates representative single-channel recordings under the control and after the addition of 100 mM LPA (upper panel) and statistical analysis of the activation in independent experiments ($n = 4$). The addition of 100 nM LPA resulted in an increase in the channel open probability from 0.79 ± 0.09 to 1.40 ± 0.45. The modulation of the ROMK2-6xHis channel activity by phosphatidic acid (PA) was also observed. The addition of 50 μg/ml PA resulted in a transient increase in the probability of opening from 0.74 ± 0.31 to 2.49 ± 0.52 ($n = 2$), followed by a decrease in the nP(o) to 0.25 ± 0.16 after approximately 3 min after compound addition ($n = 5$) (Fig. 7d). Overall, these findings suggest that the products of AGK and DGKE enzymatic activity, LPA and PA, have a significant effect on the activity of the ROMK2 channel.

3.6. The secondary anionic lipid-binding site is conserved in the ROMK2 channel

In Kir 2.1 channel two anionic lipids binding sites, primary and secondary, important for channel activation have been characterized with the primary side occupied preferentially by PIP2. However, both sites seem to bind also PA with high affinity [77]. To investigate the binding of PA to the ROMK2 channel in silico we created a homology model of the channel using the crystal structure of Kir2.2 as a template [43] (Fig. 8a) with positions of PIP2 from another Kir2.2 structure [44]. This model was equilibrated with the presence of PIP2 in its conserved binding site (Fig. 8b). Molecular docking was performed to predict the binding of the head group of PA, i.e. the methyl phosphate, to the ROMK2 protein regions involving the primary site (with and without PIP2) and the secondary site. We excluded any docking poses of PA

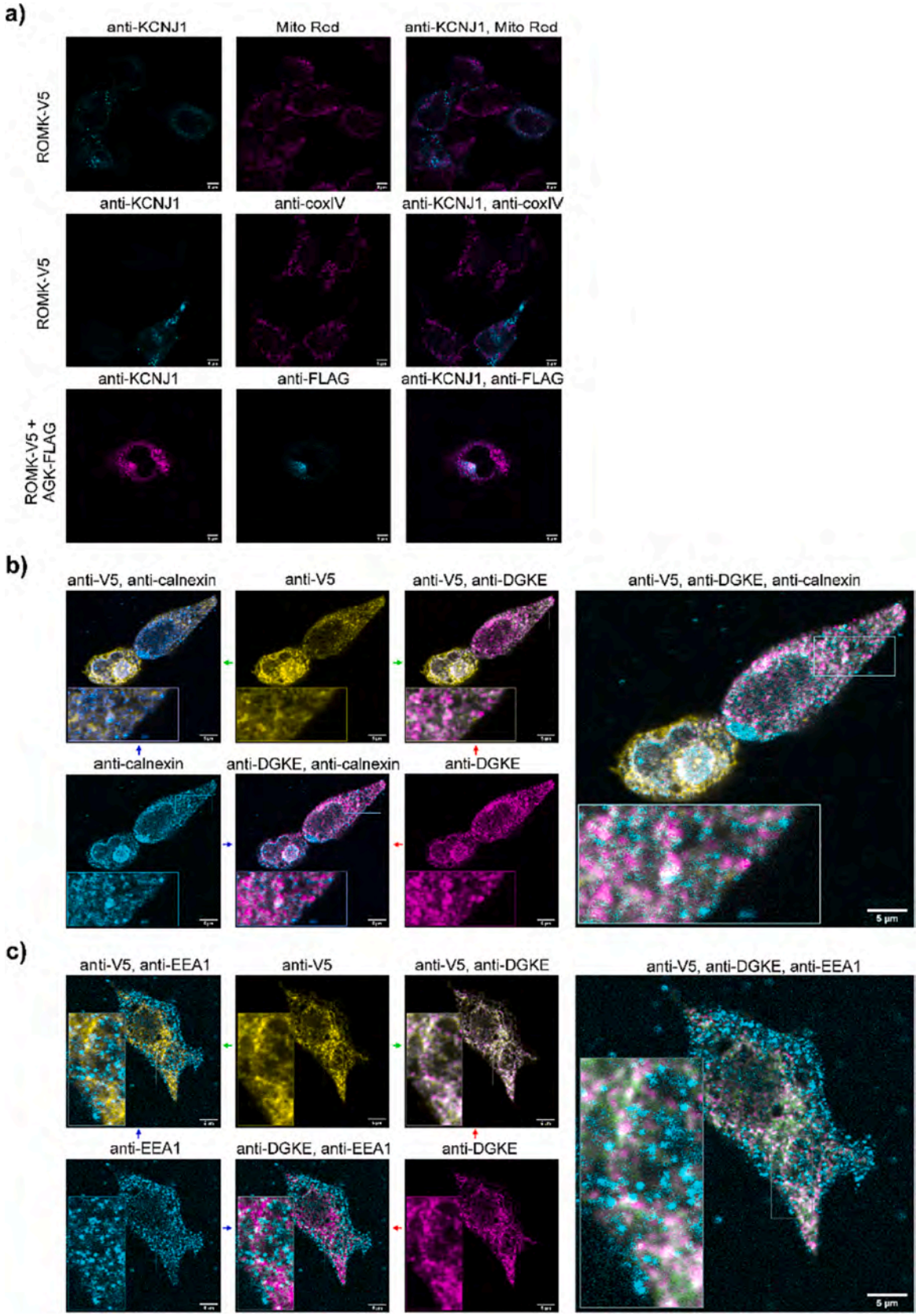

(caption on next page)

Fig. 6. Localization of the ROMK2, AGK, and DGKE proteins in HEK293T cells. a ROMK-V5 co-localization with mitochondrial markers and AGK-FLAG. Cells transfected with the plasmid pROMK2-V5 were stained with anti-KCNJ1 (1:200, Sigma Aldrich), anti-coxIV (1:200, Cell Signaling) antibodies, and also with the mitochondria-specific fluorescent dye Mito Red (100 nM, Sigma Aldrich). Cells co-transfected with plasmid pROMK2-V5 and pAGK-FLAG were stained with anti-KCNJ1 (1:200, Sigma Aldrich) and anti-FLAG (1:200, Origene) antibodies. b Co-localization of ROMK2-V5 and DGKE proteins with the endoplasmic reticulum marker calnexin. ROMK2-V5 protein was detected with anti-V5 (1:200, Sigma Aldrich). DGKE protein was labeled with anti-DGKE (1:500, Proteintech), and calnexin with anti-calnexin antibody (1:200, Abcam). Pearson's Colocalization Coefficient (PCC) was as follows - for DGKE and ROMK2 0.32, for DGKE and calnexin 0.39, and for ROMK2 and calnexin 0.36. c ROMK2-V5 and DGKE do not co-localize with the early endosome marker EEA1. PCC was as follows - for DGKE and ROMK2 0.80, for DGKE and EEA1 0.02, and for ROMK2 and EEA1 0.04. ROMK2-V5 protein was detected with anti-V5 (1:200, Sigma Aldrich), DGKE protein was labeled with anti-DGKE antibody (1:500, Proteintech), and EEA1 with anti-EEA1 antibody (1:1000, Abcam). Cells were co-transfected with pROMK2-V5 and pDGKE-FLAG plasmids (b, c).

where the methyl group of methyl phosphate, *ergo* hydrophobic tails of PA, was facing the protein or bulk water. The remaining docking poses had energies ranging from −18 kcal/mol to −16 kcal/mol and were located in distinct regions (Fig. 8a) corresponding to the primary and secondary sites. Interestingly, the secondary binding site is characterized by two positively charged residues: ARG198 and LYS199 (Fig. 8b), which are conserved among other Kir2 channels where the presence of such a secondary site was proposed (Fig. 8c) [77].

4. Discussion

Originally, ROMK2 activity was recorded in the plasma membrane [78]. In addition, ROMK2 protein has been proposed as a mitoK_{ATP} channel pore-forming subunit [19] and activity associated with ROMK2 in mitochondria was described recently [20]. Only a few proteins that interact with ROMK in the plasma membrane were found including Na^+/H^+ exchange regulatory factors, NHERF-1 and NHERF-2 as well as a clathrin adaptor protein, autosomal recessive hypercholesterolemia (ARH) [79]. NHERF binding increases cell surface expression and mediates the interaction of ROMK with CFTR regulating channel sensitivity to ligands [78,80–83]. However, there is currently no available data on proteins that interact with the ROMK channel in mitochondria and we hypothesized that ROMK2 may interact in these organelles with specific proteins potentially influencing channel function. To test this hypothesis, we aimed to identify protein partners of ROMK2 protein by proximity biotinylation using a novel variant of the promiscuous biotin ligase, TurboID [28]. Initially, we intended to conduct TurboID experiments in the H9c2 cell line, where the presence of ROMK2 in mitochondria was described [19,20]. However, we encountered difficulties with transfecting H9c2 cells at an acceptable level and decided to study the proxisome of the ROMK2 protein in HEK293T cells instead. It is worth noting that this change in the cell line may have resulted in the absence of some regulatory subunits of the ROMK2 in the present study. Also, in our studies, we did not use pure mitochondria but mitochondria-enriched intracellular membrane fractions. As a result a total of 753 proteins were identified as biotinylated by ROMK2-TurboID-3xHA. However, it is important to note that many of these proteins may have been labeled not as a result of specific interactions, but due to molecular crowding during basic cellular processes such as transcription and translation or their presence in the same cellular compartment. Indeed, it is possible to biotinylate random proteins with TurboID in "a test vial" [84]. To increase the probability of identifying specific ROMK2 partners in the mitochondrial environment, additional controls were employed. These included TurboID fusions to the targeting sequence of OTC determining TurboID localization in the mitochondrial matrix, and SMAC, which determined fusion localization in the mitochondrial intermembrane space. Both constructs colocalized well with mitochondrial markers. In the case of OTC-TurboID-3xHA, 890 proteins were identified after the purification of biotinylated proteins, whereas in the case of SMAC-TurboID-3xHA 860 proteins were identified. A large fraction of these proteins were annotated as mitochondrial (35.0 % and 35.7 % for SMAC, and OTC fusion, respectively). In contrast, only 13,1 % of the identified proteins were annotated as mitochondrial in the full ROMK2 proxisome, and among the 45 most frequently found proteins it was only 3.7 %. The largest group of identified proteins (26.6 %), among the most frequently occurring, was annotated with nuclear localization. This might be surprising, however, the presence of several ion channels [85] including several K^+ channels in nuclear membranes was reported previously [86]. The nuclear envelope is a structure that undergoes disintegration and reconstitution from the endoplasmic reticulum during cell division [87] and is continuous with ER. ROMK2 like other ion channels is inserted into ER and in agreement with that in our study, we identified in the ROMK2 proxisome four Signal Recording Particles (SRP) proteins: SRP54, SRPRA, SRPRB, and SRP68, which are involved in the co-translational transport of proteins into ER [88]. The confidence of such interactions could be increased through the use of plasmids encoding TurboID fusions targeted to individual cell compartments, as was done specifically for mitochondria. However, functional interactions for several non-mitochondrial proteins identified in the screen have already been described in the literature. One of the functional groups identified specifically in the ROMK2-TurboID-3xHA proxisome were proteins involved in clathrin-dependent endocytosis: PICALM, NOTCH1, NUMB, EPN3, CLTC, SCYL2, and PIK3C2A. Clathrin-dependent endocytosis of the ROMK2 channel has been previously described in *Xenopus oocytes* and MDCK cells [78]. It has been found that α-adaptin (AP-2), clathrin heavy chain (CLTC) [78], and the ARH protein [79] are co-immunoprecipitated with the ROMK channel. Identification of the previously known interaction with CLTC supports the specificity of the obtained results and indicates that the ROMK2 isoform is only marginally localized in mitochondria [19] and could be trafficked to and from the plasma membrane [78]. Among the identified proteins, there are also several myosins including MYO1D, MYH9, and myosin VI (MYO6). MYO6 is involved in the early stages of clathrin-dependent endocytosis in polarized epithelial cells [89]. MYH9 has been found to have a specific kidney localization in the thick ascending arm of the Henle loop [90], which is consistent with the known localization of the ROMK2 channel [25,91]. Additionally, nine proteins from the tubulin family (TUBB, TUBA1B, TUBB4B, TUBB4A, TUBA4A, TUBAL3, TUBA1A, TUBB2B, and TUBA1C) were also identified in this study. Although there have been no previous reports of interactions of the ROMK protein and tubulins, interactions between tubulins and other cationic channels, such as TRPV1 [92], EAG [93], and TRESK [94] have been documented. The presence of tubulins suggests their participation in the vesicular transport of ROMK2 [95]. The proteins mentioned above are located in the cytoplasm and play vital roles in various cellular processes, from the insertion of the protein into the ER membranes to vesicular transport and endocytosis of clathrin-coated vesicles. In addition to the structural proteins that determine transport and localization, other proteins that can directly or indirectly regulate the activity of ROMK2 have also been identified. One such protein is inosine-5′-monophosphate dehydrogenase 2 (IMPDH2), which catalyzes the NAD-dependent oxidation of inosine monophosphate (IMP) to xanthosine 5′-monophosphate (XMP), an intermediate metabolite in the production of guanosine triphosphate (GTP) [63]. IMP also serves as a substrate for ATP synthesis. As a result, IMPDH not only regulates GTP production but also ATP levels [96]. Both GTP and ATP are crucial precursors for DNA and RNA synthesis and are also fundamental to energy metabolism [62]. The ROMK2 channel's activity is inhibited by ATP [20,41], so IMPDH2 might indirectly influence the activity of ROMK2.

Several other proteins were identified only in ROMK2-TurboID-

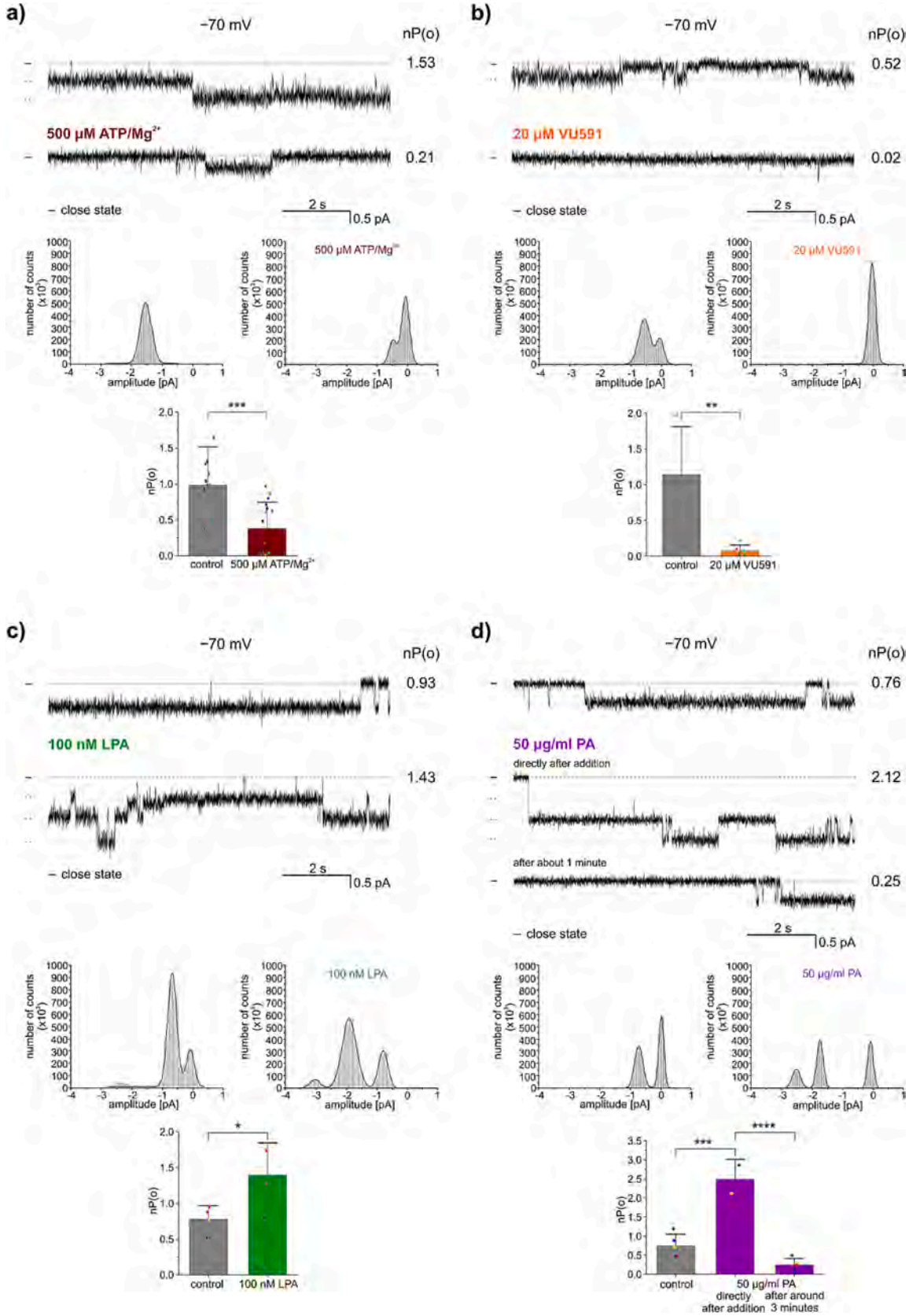

(caption on next page)

Fig. 7. Activation of ROMK2 channel by LPA and PA. a Inhibition of the activity of ROMK2 channel by ATP. *Top panel*: Representative single-channel recording of ROMK2 at −70 mV under the control conditions (upper trace) and after the addition of 500 μM ATP/Mg^{2+} (lower trace). *Middle panel:* All-point amplitude histogram for ROMK2 channel activity at −70 mV in control conditions and after the addition of 500 μM ATP/Mg^{2+}. *Lower panel*: Channel open probability, nP(o), under the control conditions and after the addition of 500 μM ATP/Mg^{2+} (n = 16).b Inhibition of the activity of ROMK2 by VU591. *Top panel*: Representative single-channel recording of ROMK2 at −70 mV under the control conditions (upper trace) and after the addition of 20 μM VU591 (lower trace). *Middle panel:* All-point amplitude histogram for ROMK2 channel activity at −70 mV in control conditions and after the addition of 20 μM VU591. *Lower panel*: Channel open probability, nP(o), under the control conditions and after the addition of 20 μM VU591 (n = 6). c Activation of ROMK2 channel by LPA. *Top panel*: Representative single-channel recording of ROMK2 at −70 mV under the control conditions (upper trace) and after the addition of 100 μM LPA (lower trace). *Middle panel:* All-point amplitude histogram for ROMK2 channel activity at −70 mV in control conditions and after the addition of 100 μM LPA. *Lower panel*: Channel open probability, nP(o), under the control conditions and after the addition of 100 μM LPA (n = 4). d Activation of ROMK2 channel by PA. *Top panel*: Representative single-channel recording of ROMK2 at −70 mV under the control conditions (upper trace) and after the addition of 50 μg/ml PA (lower trace). *Middle panel:* All-point amplitude histogram for ROMK2 channel activity at −70 mV in control conditions and after the addition of 50 μg/ml PA. *Lower panel*: Channel open probability, nP(o), under the control conditions and after the addition of 50 μg/ml PA (n = 5). -" indicates a closed state of the channel. The results related to channel open probability are presented as means ± SD.* $p < 0.05$, ** $p < 0.01$, *** $p < 0.001$, **** $p < 0.0001$. The identical ROMK2-6xHis channel preparation, as detailed in a previous study [41], was utilized. Control experiments revealed no channel activity in the absence of nanodiscs or in the presence of nanodiscs lacking the ROMK2-6xHis channel. All-point amplitude histograms (middle panels) were constructed for 30-s recordings, and traces for ten-second fragments that correspond to these recordings are illustrated in the top panels, accompanied by their respective open probabilities (nP(o)). The statistical analysis, as depicted in the lower panels, relied on nP(o) calculations derived from longer experiment-dependent recording times.

3xHA samples including peroxiredoxin 1 (PRDX1), apoptotic p53 proteins, and ADP-ribose polymerase (PARP1). These proteins can be actively transported into the mitochondria during oxidative stress [58,60,61]. Because our focus was on identifying the mitochondrial partners of ROMK2, we selected these proteins of dual-localized proteins for co-immunoprecipitation experiments. However, we were unable to demonstrate any direct interaction of ROMK2 with them. As a result, we can only hypothesize that the ROMK2 channel may be involved in signaling pathways related to DNA damage, apoptosis, or oxidative stress.

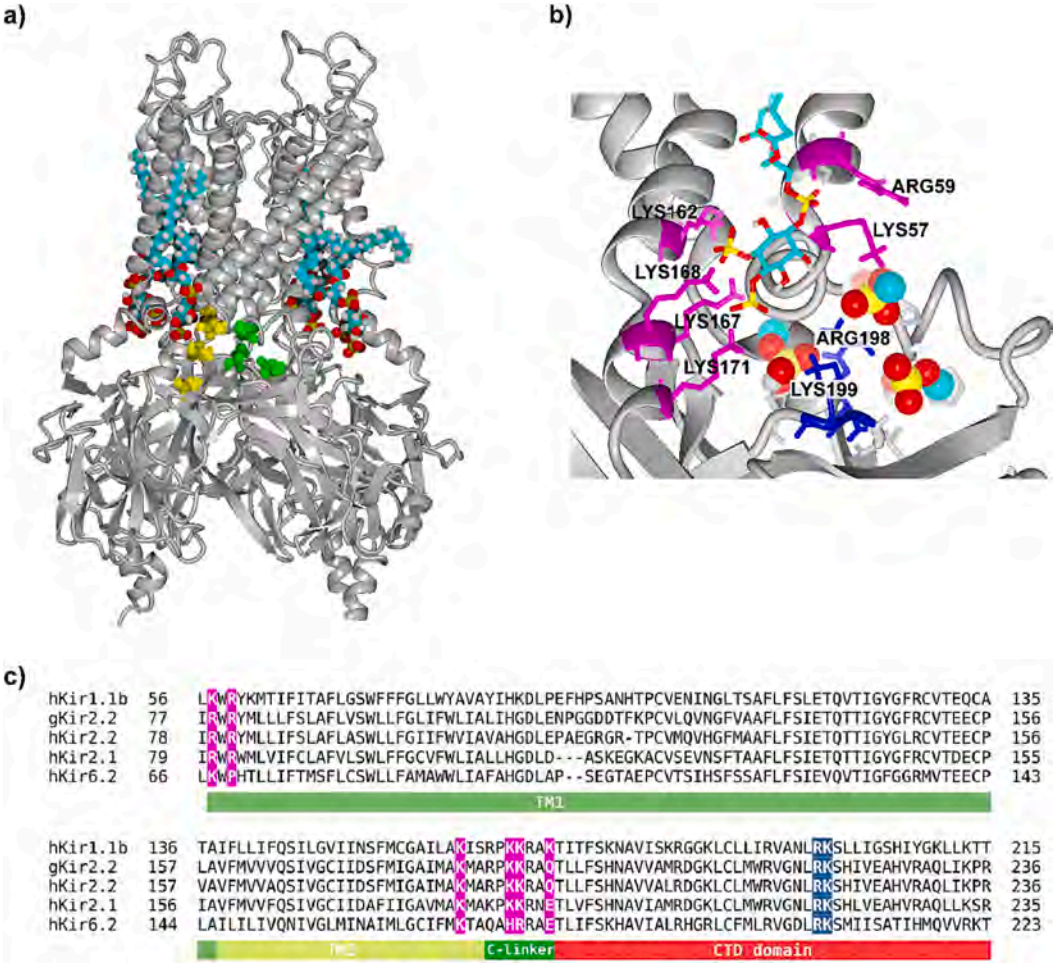

Fig. 8. Architecture of anionic lipid binding sites in ROMK2 channel. a A homology model of the ROMK2 channel is shown with four PIP2 molecules bound to each subunit (spacefill representation, colored according to the type of atom). Methyl phosphates (spacefill representation) docked in one subunit to predicted primary (yellow), and secondary (green) lipid-binding sites are shown. b A closer view of the predicted primary lipid-binding site with bound PIP2 (licorice representation colored according to the type of atom) and the secondary lipid-binding site with three docked methyl phosphates (spacefill representation, colored according to the type of atom). The figure highlights conserved amino acids important in PIP2 binding (in pink) and conserved amino acids important in anionic lipid binding in the secondary site (in blue). c A multiple sequence alignment of sequence fragments of Kir channels with highlighted positively charged residues shown in panel b with the same colors as in panel b. Structural elements are shown below the alignment.

Finally, we co-precipitated two lipid kinases, diacylglycerol kinase ε (DGKE) and acylglycerol kinase (AGK), with ROMK2. DGKE is found both in ER and cell membranes, while AGK is found in the IMM. These kinases catalyze similar reactions; DGKE phosphorylates diacylglycerol (DAG) to phosphatidic acid (PA) [117], while AGK was originally identified as a mitochondrial enzyme that phosphorylates monoacylglycerols to lysophosphatidic acids (LPA) and diacylglycerols (DAG) to phosphatidic acids (PA) [29]. Interestingly, AGK is also a subunit of the TIM22 complex [30], which is involved in the alternative import pathway of polytopic proteins [32], especially those with an odd number of transmembrane helices [98]. ROMK2 may be transported into mitochondria by either the TIM23 or TIM22 complex, similar to the transport of the yeast phosphate transporter [98]. Therefore, two non-exclusive hypotheses can be proposed: firstly, that the products of AGK's enzymatic activity may regulate the activity of the ROMK2 and secondly, the TIM22 protein complex containing AGK may import ROMK2 into the mitochondria.

Proteins are transported into mitochondria through the translocase complexes: the outer membrane translocator (TOM), and then through the inner membrane translocase (TIM) - the TIM23 and TIM22 complexes [99]. In cells transfected with pROMK2-TurboID-3xHA, among the biotinylated proteins, several other proteins involved in the import of mitochondrial precursors were also identified. Additionally, samples from cells transfected with pSMAC-TurboID-3xHA and pOTC-TurboID-3xHA revealed the identification of more proteins from these complexes. These findings are in agreement with the subcellular localization observed in microscopic images as SMAC-TurboID-3xHA and OTC-TurboID-3xHA were mainly co-localized with mitochondria, whereas only a minor fraction of ROMK2-TurboID-3xHA co-localized with these organelles.

The TOM complex proteins, including TOM5, TOM20, TOM22, TOM40 and TOM70, were identified for SMAC-TurboID-3xHA and OTC-TurboID-3xHA [100]. In contrast, in ROMK2-TurboID-3xHA samples, only TOM40, the translocase channel protein was found. The two remaining proteins of the TOM complex, i.e. TOM6 and TOM7 proteins [100] were not identified in any case. The biotinylation of TOM40 suggests the ROMK2-TurboID-3xHA may be translocated into the mitochondria. However, it cannot be ruled out that TOM40 may be labeled from the cytoplasmic side by the ROMK2-TurboID-3xHA protein located in the mitochondrial-associated membranes of the endoplasmic reticulum. On the other hand, two proteins of the TIM23 translocase complex, TIM50 and TIM44, were found to be biotinylated in the presence of ROMK2-TurboID-3xHA. TIM50 is located in the mitochondrial intermembrane space and TIM44 is located in the mitochondrial matrix [101]. In the case of SMAC-TurboID-3xHA and OTC-TurboID-3xHA, TIM50 and TIM44 proteins were detected more frequently, along with TIM16 and TIM21, which is consistent with the predominant mitochondrial localization of SMAC-TurboID-3xHA and OTC-TurboID-3xHA. The TIM23 translocase is involved in the import of both soluble and transmembrane proteins with positively charged leader sequences, which are subsequently cleaved by the MPP protease [102]. In silico analysis (BaCelLo, http://gpcr2.biocomp.unibo.it/bacello) [103] suggests that ROMK2 is localized to mitochondria, but the presence of a cleaved leader sequence necessary for the transport of ROMK2 by TIM23 translocase is unclear. Foster et al. [19] demonstrated that the ROMK2 targeting sequence (MFKHLRKWVVTRFFGHSRQRARL) directs the GFP protein to mitochondria. However, it is not known whether this sequence is cleaved by the MPP protease. Despite identifying TIM23 protein complex, the mechanism of ROMK2 transport to the IMM remains uncertain. On the other hand, except for AGK no proteins of the TIM22 complex were identified suggesting that indeed the TIM23 complex must be involved in ROMK2 insertion into the IMM. The above considerations imply that AGK does not participate in the import of ROMK2 but rather regulates its activity.

Earlier studies have shown that Kir2.1 and Kir2.2 channels are activated by PIP2, but their activity is further augmented by other anionic lipids, such as PG and PA [104]. In silico docking studies have suggested the presence of two lipid binding sites in Kir2.1 channels, including a primary PIP2 binding site and a secondary site located near the PIP2 site that is formed by two lysines, and can stabilize the PIP2 interaction upon binding with anionic lipids [77]. Our docking studies support the presence of primary and secondary anionic lipid binding sites in the ROMK channel. We found that ROMK2 activity is stimulated by LPA and PA. Unlike the previous claims that ROMK channel activity is fully dependent on PIP2 [104,105], we found that ROMK can conduct potassium ions in *E. coli* lacking PIP2 (unpublished) implying that other anionic lipids may serve as substitutes for PIP2. The roles mentioned above could potentially be fulfilled by locally synthesized LPA and PA, which are produced by AGK bound to ROMK2 in the inner mitochondrial membrane and by DGKE bound to ROMK2 in the ER (Fig. 9). A similar mechanism has been observed for the TREK-1 channel and phospholipase D2 (PLD2) [106]. It's also been hypothesized that enzymes such as diacylglycerol kinase (DAGK) and lysophosphatidic acid acyltransferase (LPAAT) could contribute to the regulation of various channels by local synthesis of PA [107]. Interestingly, in contrast to the plasma membrane, where PIP2 comprises about 1 % of total lipids [108], trace amounts of PIP2 are present in the ER [109], and PIP2 is detected only in the outer but not in the inner leaflet of IMM [110]. These PIP2-poor environments may result in the predominance of regulation of the activity of ROMK2 and other channels by PA. The physiological significance of such regulation remains to be studied. Notably, mutations of ROMK [111] and DGKE [112] have implications for the pathophysiology of the kidney and both could be involved in ischemic renal injury [113,114].

In summary, we uncovered the intracellular proximal neighborhood of the ROMK2 channel and provided evidence for the physical and functional interaction of the ROMK2 with lipid kinases in two separate subcellular compartments: AGK in mitochondria and DGKE in the endoplasmic reticulum. Further studies are needed to investigate the physiological roles of these interactions.

Funding

This work was supported by the Nencki Institute of Experimental Biology and the Polish National Science Center, grant no. 2015/19/B/NZ1/02794 (PK) and 2020/37/N/NZ1/01808 (MK). This work was also implemented as a part of Operational Project Knowledge Education Development 2014–2020 co-financed by the European Social Fund, Project No POWR.03.02.00-00-I007/16-00 (POWER 2014-2020) (MM).

Author contributions

Milena Krajewska (MK) and Piotr Koprowski (PK) designed the experiments, analyzed and interpreted data. MK performed most of the experiments and acquired data. PK contributed to plasmid design. Mariusz Możajew (MM) performed modeling and docking while Sławomir Filipek (SF) supervised these studies. PK supervised the whole project. The first draft of the manuscript was written by MK. PK revised the manuscript. All authors contributed and approved the final manuscript.

Cell lines

HEK293T cell line was kindly provided by Dr. David Stroud (University of Melbourne, Australia) 2018 and was not further authenticated.

CRediT authorship contribution statement

Milena Krajewska: Data curation, Formal analysis, Investigation, Methodology, Writing – original draft, Visualization. **Mariusz Możajew:** Investigation, Writing – review & editing, Visualization.

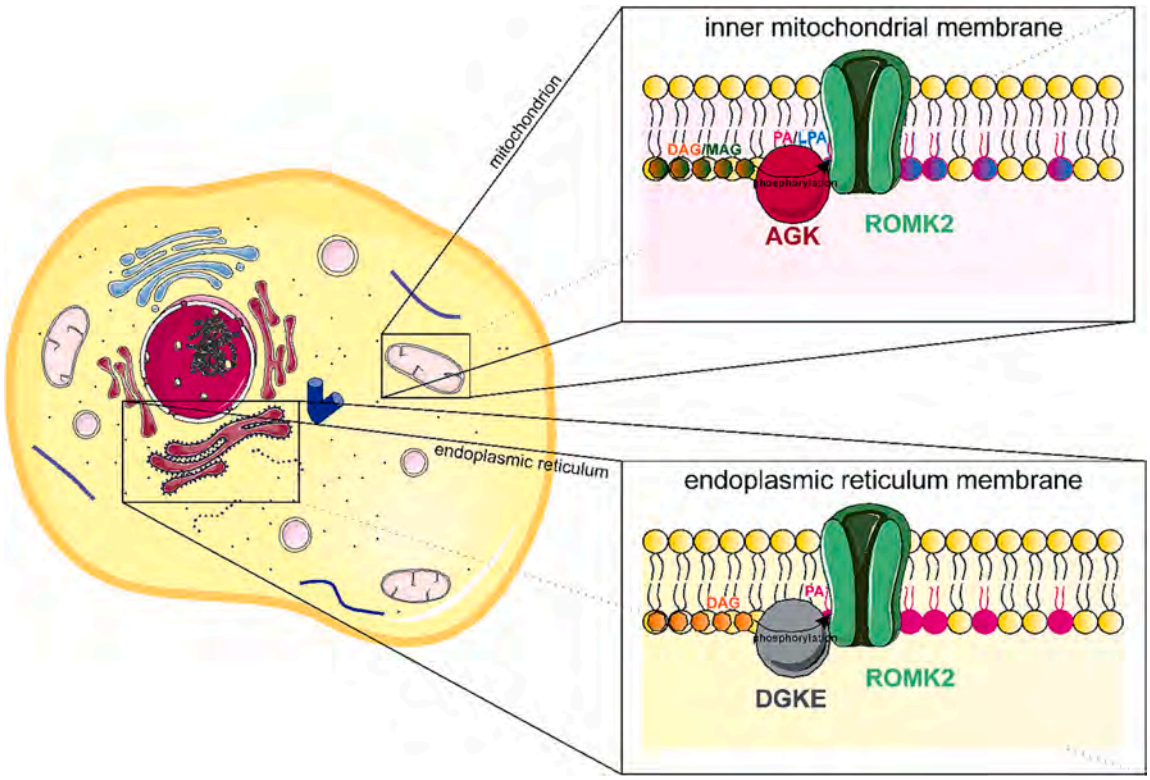

Fig. 9. Hypothetical model of ROMK2 channel regulation in low PIP2 compartments. ROMK2 channels are localized in various membrane compartments: plasma membrane, endoplasmic reticulum, and mitochondria. In high PIP2 environments, such as the plasma membrane, ROMK2 channels are primarily activated by PIP2 molecules. However, within intracellular membranes where PIP2 is scarce, ROMK2 activation occurs through a distinct mechanism. Interacting kinases AGK in mitochondria and DGKE in the endoplasmic reticulum catalyze the localized synthesis of negatively charged lipids, which then serve as activators for ROMK2 channels in these specific compartments.

Sławomir Filipek: Supervision. **Piotr Koprowski:** Conceptualization, Formal analysis, Funding acquisition, Project administration, Resources, Supervision, Validation, Writing – review & editing.

Declaration of competing interest

The authors declare no conflict of interest.

Data availability

All datasets generated during the current study are available from the corresponding author upon request.

Acknowledgments

We would like to thank Polyscope Polymers (Netherlands) for providing the SMA copolymers: Xiran® SL30010 P20 (SMA 2.3:1) and Mr. Robert Zonko (BASF Poland) for providing Sokalan® CP9.

We would like to thank dr Bogusz Kulawiak (Nencki Institute of Experimental Biology) for fruitful discussions. We would like to thank dr Przemysław Miszta (Faculty of Chemistry, University of Warsaw) for the help with docking studies.

The equipment used for MS analyses was sponsored in part by the Centre for Preclinical Research and Technology (CePT), a project co-sponsored by the European Regional Development Fund and Innovative Economy, The National Cohesion Strategy of Poland.

Appendix A. Supplementary data

Supplementary data to this article can be found online at https://doi.org/10.1016/j.bbalip.2023.159443.

References

[1] B. O'Rourke, Mitochondrial ion channels, Annu. Rev. Physiol. 69 (2007) 19–49, https://doi.org/10.1146/annurev.physiol.69.031905.163804.
[2] I. Inoue, H. Nagase, K. Kishi, T. Higuti, ATP-sensitive K^+ channel in the mitochondrial inner membrane, Nature 352 (1991) 244–247, https://doi.org/10.1038/352244a0.
[3] P. Paucek, G. Mironova, F. Mahdi, A.D. Beavis, G. Woldegiorgis, K.D. Garlid, Reconstitution and partial purification of the glibenclamide-sensitive, ATP-dependent K^+ channel from rat liver and beef heart mitochondria, J. Biol. Chem. 267 (1992) 26062–26069, https://doi.org/10.1016/s0021-9258(18)35717-x.
[4] D.V. Cancherini, L.G. Trabuco, N.A. Reboucas, A.J. Kowaltowski, ATP-sensitive K^+ channels in renal mitochondria, Am. J. Physiol. Renal Physiol. 285 (2003) F1291–F1296, https://doi.org/10.1152/ajprenal.00103.2003.
[5] R. Bajgar, S. Seetharaman, A.J. Kowaltowski, K.D. Garlid, P. Paucek, Identification and properties of a novel intracellular (mitochondrial) ATP-sensitive potassium channel in brain, J. Biol. Chem. 276 (2001) 33369–33374, https://doi.org/10.1074/jbc.M103320200.
[6] G. Debska, R. May, A. Kicinska, A. Szewczyk, C.E. Elger, W.S. Kunz, Potassium channel openers depolarize hippocampal mitochondria, Brain Res. 892 (2001) 42–50, https://doi.org/10.1016/s0006-8993(00)03187-5.
[7] G. Debska, A. Kicinska, J. Skalska, A. Szewczyk, R. May, C.E. Elger, W.S. Kunz, Opening of potassium channels modulates mitochondrial function in rat skeletal muscle, Biochim. Biophys. Acta 1556 (2002) 97–105, https://doi.org/10.1016/s0005-2728(02)00340-7.
[8] Y.A. Dahlem, T.F. Horn, L. Buntinas, T. Gonoi, G. Wolf, D. Siemen, The human mitochondrial K_{ATP} channel is modulated by calcium and nitric oxide: a patch-clamp approach, Biochim. Biophys. Acta 1656 (2004) 46–56, https://doi.org/10.1016/j.bbabio.2004.01.003.
[9] A. Paggio, V. Checchetto, A. Campo, R. Menabo, G. Di Marco, F. Di Lisa, I. Szabo, R. Rizzuto, D. De Stefani, Identification of an ATP-sensitive potassium channel in mitochondria, Nature 572 (2019) 609–613, https://doi.org/10.1038/s41586-019-1498-3.
[10] P. Bednarczyk, A. Kicinska, M. Laskowski, B. Kulawiak, R. Kampa, A. Walewska, M. Krajewska, W. Jarmuszkiewicz, A. Szewczyk, Evidence for a mitochondrial ATP-regulated potassium channel in human dermal fibroblasts, Biochim. Biophys. Acta Bioenerg. 2018 (1859) 309–318, https://doi.org/10.1016/j.bbabio.2018.02.005.
[11] K. Choma, P. Bednarczyk, I. Koszela-Piotrowska, B. Kulawiak, A. Kudin, W. S. Kunz, K. Dolowy, A. Szewczyk, Single channel studies of the ATP-regulated

potassium channel in brain mitochondria, J. Bioenerg. Biomembr. 41 (2009) 323–334, https://doi.org/10.1007/s10863-009-9233-7.
[12] G.D. Mironova, Y.Y. Skarga, S.M. Grigoriev, A.E. Negoda, O.V. Kolomytkin, B. S. Marinov, Reconstitution of the mitochondrial ATP-dependent Potassium Channel into bilayer lipid Membrane1, J. Bioenerg. Biomembr. 31 (1999) 159–163, https://doi.org/10.1023/A:1005408029549.
[13] D.X. Zhang, Y.F. Chen, W.B. Campbell, A.P. Zou, G.J. Gross, P.L. Li, Characteristics and superoxide-induced activation of reconstituted myocardial mitochondrial ATP-sensitive potassium channels, Circ. Res. 89 (2001) 1177–1183, https://doi.org/10.1161/hh2401.101752.
[14] P. Bednarczyk, K. Dolowy, A. Szewczyk, Matrix Mg^{2+} regulates mitochondrial ATP-dependent potassium channel from heart, FEBS Lett. 579 (2005) 1625–1632, https://doi.org/10.1016/j.febslet.2005.01.077.
[15] P. Bednarczyk, K. Dolowy, A. Szewczyk, New properties of mitochondrial ATP-regulated potassium channels, J. Bioenerg. Biomembr. 40 (2008) 325–335, https://doi.org/10.1007/s10863-008-9153-y.
[16] K.D. Garlid, P. Paucek, V. Yarov-Yarovoy, X. Sun, P.A. Schindler, The mitochondrial K_{ATP} channel as a receptor for potassium channel openers, J. Biol. Chem. 271 (1996) 8796–8799, https://doi.org/10.1074/jbc.271.15.8796.
[17] Y. Liu, T. Sato, B. O'Rourke, E. Marban, Mitochondrial ATP-dependent potassium channels: novel effectors of cardioprotection? Circulation 97 (1998) 2463–2469, https://doi.org/10.1161/01.CIR.97.24.2463.
[18] J. Fahanik-Babaei, A. Eliassi, R. Saghiri, Biophysical and electropharmacological properties of single mitoK_{ATP} channel in rat brain mitochondrial inner membrane, Physiol Pharmacol 16 (2012) 283–299.
[19] D.B. Foster, A.S. Ho, J. Rucker, A.O. Garlid, L. Chen, A. Sidor, K.D. Garlid, B. O'Rourke, Mitochondrial ROMK channel is a molecular component of mitoK_{ATP}, Circ. Res. 111 (2012) 446–454, https://doi.org/10.1161/CIRCRESAHA.112.266445.
[20] M. Laskowski, B. Augustynek, P. Bednarczyk, M. Zochowska, J. Kalisz, B. O'Rourke, A. Szewczyk, B. Kulawiak, Single-channel properties of the ROMK-pore-forming subunit of the mitochondrial ATP-sensitive potassium channel, Int. J. Mol. Sci. 20 (2019) 5323, https://doi.org/10.3390/ijms20215323.
[21] K.N. Papanicolaou, D. Ashok, T. Liu, T.M. Bauer, J. Sun, Z. Li, E. da Costa, C. C. D'Orleans, S. Nathan, D.J. Lefer, E. Murphy, N. Paolocci, D.B. Foster, B. O'Rourke, Global knockout of ROMK potassium channel worsens cardiac ischemia-reperfusion injury but cardiomyocyte-specific knockout does not: implications for the identity of mitoK_{ATP}, J. Mol. Cell. Cardiol. 139 (2020) 176–189, https://doi.org/10.1016/j.yjmcc.2020.01.010.
[22] S. Chepilko, H. Zhou, H. Sackin, L.G. Palmer, Permeation and gating properties of a cloned renal K^+ channel, Am. J. Physiol. 268 (1995) C389–C401, https://doi.org/10.1152/ajpcell.1995.268.2.C389.
[23] C.M. McNicholas, W.B. Guggino, E.M. Schwiebert, S.C. Hebert, G. Giebisch, M. E. Egan, Sensitivity of a renal K^+ channel (ROMK2) to the inhibitory sulfonylurea compound glibenclamide is enhanced by coexpression with the ATP-binding cassette transporter cystic fibrosis transmembrane regulator, Proc. Natl. Acad. Sci. U. S. A. 93 (1996) 8083–8088, https://doi.org/10.1073/pnas.93.15.808.
[24] H. Hibino, A. Inanobe, K. Furutani, S. Murakami, I. Findlay, Y. Kurachi, Inwardly rectifying potassium channels: their structure, function, and physiological roles, Physiol. Rev. 90 (2010) 291–366, https://doi.org/10.1152/physrev.00021.2009.
[25] P.A. Welling, K. Ho, A comprehensive guide to the ROMK potassium channel: form and function in health and disease, Am. J. Physiol. Renal Physiol. 297 (2009) F849–F863, https://doi.org/10.1152/ajprenal.00181.2009.
[26] L. Aguilar-Bryan, J. Bryan, Molecular biology of adenosine triphosphate-sensitive potassium channel, Endocr. Rev. 20 (1999) 101–135, https://doi.org/10.1210/edrv.20.2.0361.
[27] X. Liu, B.B. Singh, I.S. Ambudkar, ATP-dependent activation of K_{Ca} and ROMK-type K_{ATP} channels in human submandibular gland ductal cells, J. Biol. Chem. 274 (1999) 25121–25129, https://doi.org/10.1074/jbc.274.35.25121.
[28] T.C. Branon, J.A. Bosch, A.D. Sanchez, N.D. Udeshi, T. Svinkina, S.A. Carr, J. L. Feldman, N. Perrimon, A.Y. Ting, Efficient proximity labeling in living cells and organisms with TurboID, Nat. Biotechnol. 36 (2018) 880–887, https://doi.org/10.1038/nbt.4201.
[29] M. Bektas, S.G. Payne, H. Liu, S. Goparaju, S. Milstien, S. Spiegel, A novel acylglycerol kinase that produces lysophosphatidic acid modulates cross talk with EGFR in prostate cancer cells, J. Cell Biol. 169 (2005) 801–811, https://doi.org/10.1083/jcb.200407123.
[30] M. Vukotic, H. Nolte, T. König, S. Saita, M. Ananjew, M. Krüger, T. Tatsuta, T. Langer, Acylglycerol kinase mutated in sengers syndrome is a subunit of the TIM22 protein translocase in mitochondria, Mol. Cell 67 (2017) 471–483.e477, https://doi.org/10.1016/j.molcel.2017.06.013.
[31] Y. Kang, D.A. Stroud, M.J. Baker, D.P. De Souza, A.E. Frazier, M. Liem, D. Tull, S. Mathivanan, M.J. McConville, D.R. Thorburn, M.T. Ryan, D. Stojanovski, Sengers syndrome-associated mitochondrial acylglycerol kinase is a subunit of the human TIM22 protein import complex, Mol. Cell 67 (2017) 457–470 e455, https://doi.org/10.1016/j.molcel.2017.06.014.
[32] T.D. Jackson, D.H. Hock, K.M. Fujihara, C.S. Palmer, A.E. Frazier, Y.C. Low, Y. Kang, C.S. Ang, N.J. Clemons, D.R. Thorburn, D.A. Stroud, D. Stojanovski, The TIM22 complex mediates the import of sideroflexins and is required for efficient mitochondrial one-carbon metabolism, Mol. Biol. Cell 32 (2021) 475–491, https://doi.org/10.1091/mbc.E20-06-0390.
[33] N. Kobayashi, Y. Hozumi, T. Ito, T. Hosoya, H. Kondo, K. Goto, Differential subcellular targeting and activity-dependent subcellular localization of diacylglycerol kinase isozymes in transfected cells, Eur. J. Cell Biol. 86 (2007) 433–444, https://doi.org/10.1016/j.ejcb.2007.05.002.
[34] S.W. Tait, M.J. Parsons, F. Llambi, L. Bouchier-Hayes, S. Connell, C. Munoz-Pinedo, D.R. Green, Resistance to caspase-independent cell death requires persistence of intact mitochondria, Dev. Cell 18 (2010) 802–813, https://doi.org/10.1016/j.devcel.2010.03.014.
[35] Q. Zhao, J. Wang, I.V. Levivhkin, S. Stasinopoulos, M.T. Ryan, N.J. Hoogenraad, A mitochondrial specific stress response in mammalian cells, EMBO J. 21 (2002) 4411–4419, https://doi.org/10.1093/emboj/cdf445.
[36] G. Sarkar, S.S. Sommer, The "megaprimer" method of site-directed mutagenesis, Biotechniques 8 (1990) 404–407.
[37] A.P. Kudin, N.Y. Bimpong-Buta, S. Vielhaber, C.E. Elger, W.S. Kunz, Characterization of superoxide-producing sites in isolated brain mitochondria, J. Biol. Chem. 279 (2004) 4127–4135, https://doi.org/10.1074/jbc.M310341200.
[38] P. Bednarczyk, M.R. Wieckowski, M. Broszkiewicz, K. Skowronek, D. Siemen, A. Szewczyk, Putative structural and functional coupling of the mitochondrial BK_{Ca} channel to the respiratory chain, PloS One 8 (2013), e68125, https://doi.org/10.1371/journal.pone.0068125.
[39] K.J. Roux, D.I. Kim, B. Burke, BioID: a screen for protein-protein interactions, Curr. Protoc. Protein Sci. 74 (2013), https://doi.org/10.1002/0471140864.ps1923s74, 19.23.1-19.23.14.
[40] K. Lin, Q. Yan, A. Mitchell, N. Funk, C. Lu, H. Xiao, A simple method for non-denaturing purification of biotin-tagged proteins through competitive elution with free biotin, Biotechniques 68 (2020) 41–44, https://doi.org/10.2144/btn-2019-0088.
[41] M. Krajewska, P. Koprowski, Solubilization, purification, and functional reconstitution of human ROMK potassium channel in copolymer styrene-maleic acid (SMA) nanodiscs, Biochim. Biophys. Acta Biomembr. 1863 (2021), 183555, https://doi.org/10.1016/j.bbamem.2021.183555.
[42] A. Waterhouse, M. Bertoni, S. Bienert, G. Studer, G. Tauriello, R. Gumienny, F. T. Heer, T.A.P. de Beer, C. Rempfer, L. Bordoli, R. Lepore, T. Schwede, SWISS-MODEL: homology modelling of protein structures and complexes, Nucleic Acids Res. 46 (2018) W296–W303, https://doi.org/10.1093/nar/gky427.
[43] S.J. Lee, F. Ren, E.M. Zangerl-Plessl, S. Heyman, A. Stary-Weinzinger, P. Yuan, C. G. Nichols, Structural basis of control of inward rectifier Kir2 channel gating by bulk anionic phospholipids, J. Gen. Physiol. 148 (2016) 227–237, https://doi.org/10.1085/jgp.201611616.
[44] S.B. Hansen, X. Tao, R. MacKinnon, Structural basis of PIP2 activation of the classical inward rectifier K+ channel Kir2.2, Nature 477 (2011) 495–498, https://doi.org/10.1038/nature10370.
[45] W. Humphrey, A. Dalke, K. Schulten, VMD: visual molecular dynamics, J. Mol. Graph. 14 (1996) 33–38, https://doi.org/10.1016/0263-7855(96)00018-5.
[46] J.C. Phillips, D.J. Hardy, J.D.C. Maia, J.E. Stone, J.V. Ribeiro, R.C. Bernardi, R. Buch, G. Fiorin, J. Hénin, W. Jiang, R. McGreevy, M.C.R. Melo, B.K. Radak, R. D. Skeel, A. Singharoy, Y. Wang, B. Roux, A. Aksimentiev, Z. Luthey-Schulten, L. V. Kalé, K. Schulten, C. Chipot, E. Tajkhorshid, Scalable molecular dynamics on CPU and GPU architectures with NAMD, J. Chem. Phys. 153 (2020), 044130, https://doi.org/10.1063/5.0014475.
[47] J.B. Klauda, R.M. Venable, J.A. Freites, J.W. O'Connor, D.J. Tobias, C. Mondragon-Ramirez, I. Vorobyov, A.D. MacKerell Jr., R.W. Pastor, Update of the CHARMM all-atom additive force field for lipids: validation on six lipid types, J. Phys. Chem. B 114 (2010) 7830–7843, https://doi.org/10.1021/jp101759q.
[48] K. Vanommeslaeghe, E.P. Raman, A.D. MacKerell Jr., Automation of the CHARMM general force field (CGenFF) II: assignment of bonded parameters and partial atomic charges, J. Chem. Inf. Model. 52 (2012) 3155–3168, https://doi.org/10.1021/ci3003649.
[49] U. Essmann, L. Perera, M.L. Berkowitz, T. Darden, H. Lee, L.G. Pedersen, A smooth particle mesh Ewald method, J. Chem. Phys. 103 (1995) 8577–8593, https://doi.org/10.1063/1.470117.
[50] J. An, M. Totrov, R. Abagyan, Pocketome via comprehensive identification and classification of ligand binding envelopes, Mol. Cell. Proteomics 4 (2005) 752–761, https://doi.org/10.1074/mcp.M400159-MCP200.
[51] R. Abagyan, M. Totrov, Biased probability Monte Carlo conformational searches and electrostatic calculations for peptides and proteins, J. Mol. Biol. 235 (1994) 983–1002, https://doi.org/10.1006/jmbi.1994.1052.
[52] T.C. Branon, J.A. Bosch, A.D. Sanchez, N.D. Udeshi, T. Svinkina, S.A. Carr, J. L. Feldman, N. Perrimon, A.Y. Ting, Directed evolution of TurboID for efficient proximity labeling in living cells and organisms, Nat. Biotechnol. 36 (2017) 880–887, https://doi.org/10.1101/196980.
[53] A.L. Horwich, F. Kalousek, W.A. Fenton, R.A. Pollock, L.E. Rosenberg, Targeting of pre-ornithine transcarbamylase to mitochondria: definition of critical regions and residues in the leader peptide, Cell 44 (1986) 451–459, https://doi.org/10.1016/0092-8674(86)90466-6.
[54] A.L. Horwich, F. Kalousek, L.E. Rosenberg, Arginine in the leader peptide is required for both import and proteolytic cleavage of a mitochondrial precursor, Proc. Natl. Acad. Sci. U. S. A. 82 (1985) 4930–4933, https://doi.org/10.1073/pnas.82.15.4930.
[55] R.Y. Wang, W.R. Wilcox, S.D. Cederbaum, Chapter 92 - amino acid metabolism, in: D. Rimoin, R. Pyeritz, B. Korf (Eds.), Emery and Rimoin's Principles and Practice of Medical Genetics, Academic Press, Oxford, 2013, pp. 1–42.
[56] C. Du, M. Fang, Y. Li, L. Li, X. Wang, Smac, a mitochondrial protein that promotes cytochrome c-dependent caspase activation by eliminating IAP inhibition, Cell 102 (2000) 33–42, https://doi.org/10.1016/S0092-8674(00)00008-8.
[57] J. Fu, Y. Jin, L.J. Arend, Smac3, a novel Smac/DIABLO splicing variant, attenuates the stability and apoptosis-inhibiting activity of X-linked inhibitor of apoptosis protein, J. Biol. Chem. 278 (2003) 52660–52672, https://doi.org/10.1074/jbc.M308036200.

[58] P. Bai, L. Nagy, T. Fodor, L. Liaudet, P. Pacher, Poly(ADP-ribose) polymerases as modulators of mitochondrial activity, Trends Endocrinol. Metab. 26 (2015) 75–83, https://doi.org/10.1016/j.tem.2014.11.003.
[59] A.V. Vaseva, N.D. Marchenko, K. Ji, S.E. Tsirka, S. Holzmann, U.M. Moll, p53 opens the mitochondrial permeability transition pore to trigger necrosis, Cell 149 (2012) 1536–1548, https://doi.org/10.1016/j.cell.2012.05.014.
[60] Y. Zhao, L. Chaiswing, J.M. Velez, I. Batinic-Haberle, N.H. Colburn, T.D. Oberley, D.K.S. Clair, p53 translocation to mitochondria precedes its nuclear translocation and targets mitochondrial oxidative defense protein-manganese superoxide dismutase, Cancer Res. 65 (2005) 3745–3750, https://doi.org/10.1158/0008-5472.CAN-04-3835.
[61] N. Noda, R. Awais, R. Sutton, M. Awais, T. Ozawa, Dynamic monitoring of p53 translocation to mitochondria for the analysis of specific inhibitors using luciferase-fragment complementation, Biotechnol. Bioeng. 114 (2017) 2818–2827, https://doi.org/10.1002/bit.26407.
[62] R. Naffouje, P. Grover, H. Yu, A. Sendilnathan, K. Wolfe, N. Majd, E.P. Smith, K. Takeuchi, T. Senda, S. Kofuji, A.T. Sasaki, Anti-tumor potential of IMP dehydrogenase inhibitors: a century-Long story, Cancers (Basel) 11 (2019) 1346, https://doi.org/10.3390/cancers11091346.
[63] J.E. McLean, N. Hamaguchi, P. Belenky, S.E. Mortimer, M. Stanton, L. Hedstrom, Inosine 5′-monophosphate dehydrogenase binds nucleic acids in vitro and in vivo, Biochem. J. 379 (2004) 243–251, https://doi.org/10.1042/bj20031585.
[64] H. Kaneko, H. Kitoh, T. Matsuura, A. Masuda, M. Ito, M. Mottes, F. Rauch, N. Ishiguro, K. Ohno, Hyperuricemia cosegregating with osteogenesis imperfecta is associated with a mutation in GPATCH8, Hum. Genet. 130 (2011) 671–683, https://doi.org/10.1007/s00439-011-1006-9.
[65] A.R. Long, C.C. O'Brien, K. Malhotra, C.T. Schwall, A.D. Albert, A. Watts, N. N. Alder, A detergent-free strategy for the reconstitution of active enzyme complexes from native biological membranes into nanoscale discs, BMC Biotechnol. 13 (2013) 41, https://doi.org/10.1186/1472-6750-13-41.
[66] S. Paulin, M. Jamshad, T.R. Dafforn, J. Garcia-Lara, S.J. Foster, N.F. Galley, D. I. Roper, H. Rosado, P.W. Taylor, Surfactant-free purification of membrane protein complexes from bacteria: application to the staphylococcal penicillin-binding protein complex PBP2/PBP2a, Nanotechnology 25 (2014), 285101, https://doi.org/10.1088/0957-4484/25/28/285101.
[67] D.J.K. Swainsbury, M.S. Proctor, A. Hitchcock, M.L. Cartron, P. Qian, E.C. Martin, P.J. Jackson, J. Madsen, S.P. Armes, C.N. Hunter, Probing the local lipid environment of the *Rhodobacter sphaeroides* cytochrome bc1 and *Synechocystis* sp. PCC 6803 cytochrome b6f complexes with styrene maleic acid, Biochim Biophys Acta Bioenerg 1859 (2018) 215–225, https://doi.org/10.1016/j.bbabio.2017.12.005.
[68] A. Desrames, S. Genetet, M.P. Delcourt, D. Goossens, I. Mouro-Chanteloup, Detergent-free isolation of native red blood cell membrane complexes, Biochim Biophys Acta Biomembr 1862 (2020), 183126, https://doi.org/10.1016/j.bbamem.2019.183126.
[69] I.A. Smirnova, D. Sjostrand, F. Li, M. Bjorck, J. Schafer, H. Ostbye, M. Hogbom, C. von Ballmoos, G.C. Lander, P. Adelroth, P. Brzezinski, Isolation of yeast complex IV in native lipid nanodiscs, Biochim. Biophys. Acta 2016 (1858) 2984–2992, https://doi.org/10.1016/j.bbamem.2016.09.004.
[70] C. Sun, S. Benlekbir, P. Venkatakrishnan, Y. Wang, S. Hong, J. Hosler, E. Tajkhorshid, J.L. Rubinstein, R.B. Gennis, Structure of the alternative complex III in a supercomplex with cytochrome oxidase, Nature 557 (2018) 123–126, https://doi.org/10.1038/s41586-018-0061-y.
[71] S.C. Lee, R. Collins, Y.P. Lin, M. Jamshad, C. Broughton, S.A. Harris, B.S. Hanson, C. Tognoloni, R.A. Parslow, A.E. Terry, A. Rodger, C.J. Smith, K.J. Edler, R. Ford, D.I. Roper, T.R. Dafforn, Nano-encapsulated *Escherichia coli* Divisome anchor ZipA, and in complex with FtsZ, Sci. Rep. 9 (2019) 18712, https://doi.org/10.1038/s41598-019-54999-x.
[72] A. Kicinska, A. Swida, P. Bednarczyk, I. Koszela-Piotrowska, K. Choma, K. Dolowy, A. Szewczyk, W. Jarmuszkiewicz, ATP-sensitive potassium channel in mitochondria of the eukaryotic microorganism *Acanthamoeba castellanii*, J. Biol. Chem. 282 (2007) 17433–17441, https://doi.org/10.1074/jbc.M701496200.
[73] P. Bednarczyk, A. Kicinska, M. Laskowski, B. Kulawiak, R. Kampa, A. Walewska, M. Krajewska, W. Jarmuszkiewicz, A. Szewczyk, Evidence for a mitochondrial ATP-regulated potassium channel in human dermal fibroblasts, Biochim. Biophys. Acta Bioenerg. 2018 (1859) 309–318, https://doi.org/10.1016/j.bbabio.2018.02.005.
[74] C.M. McNicholas, Y. Yang, G. Giebisch, S.C. Hebert, Molecular site for nucleotide binding on an ATP-sensitive renal K^+ channel (ROMK2), Am. J. Physiol. 271 (1996) F275–F285, https://doi.org/10.1152/ajprenal.1996.271.2.F275.
[75] G. Bhave, B.A. Chauder, W. Liu, E.S. Dawson, R. Kadakia, T.T. Nguyen, L. M. Lewis, J. Meiler, C.D. Weaver, L.M. Satlin, C.W. Lindsley, J.S. Denton, Development of a selective small-molecule inhibitor of Kir1.1, the renal outer medullary potassium channel, Mol. Pharmacol. 79 (2011) 42–50, https://doi.org/10.1124/mol.110.066928.
[76] D.R. Swale, J.H. Sheehan, S. Banerjee, A.S. Husni, T.T. Nguyen, J. Meiler, J. S. Denton, Computational and functional analyses of a small-molecule binding site in ROMK, Biophys. J. 108 (2015) 1094–1103, https://doi.org/10.1016/j.bpj.2015.01.022.
[77] S.J. Lee, S. Wang, W. Borschel, S. Heyman, J. Gyore, C.G. Nichols, Secondary anionic phospholipid binding site and gating mechanism in Kir2.1 inward rectifier channels, Nat. Commun. 4 (2013) 2786, https://doi.org/10.1038/ncomms3786.
[78] W.Z. Zeng, V. Babich, B. Ortega, R. Quigley, S.J. White, P.A. Welling, C.L. Huang, Evidence for endocytosis of ROMK potassium channel via clathrin-coated vesicles, Am. J. Physiol. Renal Physiol. 283 (2002) F630–F639, https://doi.org/10.1152/ajprenal.00378.2001.
[79] L. Fang, R. Garuti, B.Y. Kim, J.B. Wade, P.A. Welling, The ARH adaptor protein regulates endocytosis of the ROMK potassium secretory channel in mouse kidney, J. Clin. Invest. 119 (2009) 3278–3289, https://doi.org/10.1172/jci37950.
[80] D. Yoo, T.P. Flagg, O. Olsen, V. Raghuram, J.K. Foskett, P.A. Welling, Assembly and trafficking of a multiprotein ROMK (Kir 1.1) channel complex by PDZ interactions, J. Biol. Chem. 279 (2004) 6863–6873, https://doi.org/10.1074/jbc.M311599200.
[81] M. Lu, Q. Leng, M.E. Egan, M.J. Caplan, E.L. Boulpaep, G.H. Giebisch, S. C. Hebert, CFTR is required for PKA-regulated ATP sensitivity of Kir1.1 potassium channels in mouse kidney, J. Clin. Invest. 116 (2006) 797–807, https://doi.org/10.1172/JCI26961.
[82] A. Ruknudin, D.H. Schulze, S.K. Sullivan, W.J. Lederer, P.A. Welling, Novel subunit composition of a renal epithelial K_{ATP} channel, J. Biol. Chem. 273 (1998) 14165–14171, https://doi.org/10.1074/jbc.273.23.14165.
[83] D.B. Simon, F.E. Karet, J. Rodriguez-Soriano, J.H. Hamdan, A. DiPietro, H. Trachtman, S.A. Sanjad, R.P. Lifton, Genetic heterogeneity of Bartter's syndrome revealed by mutations in the K^+ channel, ROMK, Nat. Genet. 14 (1996) 152–156, https://doi.org/10.1038/ng1096-152.
[84] R. Shioya, K. Yamada, K. Kido, H. Takahashi, A. Nozawa, H. Kosako, T. Sawasaki, A simple method for labeling proteins and antibodies with biotin using the proximity biotinylation enzyme TurboID, Biochem. Biophys. Res. Commun. 592 (2022) 54–59, https://doi.org/10.1016/j.bbrc.2021.12.109.
[85] D. Anand, A. Chaudhuri, Grease in the nucleus: insights into the dynamic life of nuclear membranes, J. Membr. Biol. (2022), https://doi.org/10.1007/s00232-022-00272-8.
[86] J. Capera, C. Serrano-Novillo, M. Navarro-Pérez, S. Cassinelli, A. Felipe, The potassium channel odyssey: mechanisms of traffic and membrane arrangement, Int. J. Mol. Sci. 20 (2019) 734, https://doi.org/10.3390/ijms20030734.
[87] A.R. English, G.K. Voeltz, Endoplasmic reticulum structure and interconnections with other organelles, Cold Spring Harb. Perspect. Biol. 5 (2013), a013227, https://doi.org/10.1101/cshperspect.a013227.
[88] E.A. Costa, K. Subramanian, J. Nunnari, J.S. Weissman, Defining the physiological role of SRP in protein-targeting efficiency and specificity, Science 359 (2018) 689–692, https://doi.org/10.1126/science.aar3607.
[89] F. Buss, S.D. Arden, M. Lindsay, J.P. Luzio, J. Kendrick-Jones, Myosin VI isoform localized to clathrin-coated vesicles with a role in clathrin-mediated endocytosis, EMBO J. 20 (2001) 3676–3684, https://doi.org/10.1093/emboj/20.14.3676.
[90] K.L. Otterpohl, R.G. Hart, C. Evans, K. Surendran, I. Chandrasekar, Nonmuscle myosin 2 proteins encoded by Myh9, Myh10, and Myh14 are uniquely distributed in the tubular segments of murine kidney, Physiol. Rep. 5 (2017), e13513, https://doi.org/10.14814/phy2.13513.
[91] C.A. Ecelbarger, G.H. Kim, M.A. Knepper, J. Liu, M. Tate, P.A. Welling, J.B. Wade, Regulation of potassium channel Kir 1.1 (ROMK) abundance in the thick ascending limb of Henle's loop, J. Am. Soc. Nephrol. 12 (2001) 10–18, https://doi.org/10.1681/asn.V12110.
[92] C. Goswami, M. Dreger, R. Jahnel, O. Bogen, C. Gillen, F. Hucho, Identification and characterization of a Ca^{2+}-sensitive interaction of the vanilloid receptor TRPV1 with tubulin, J. Neurochem. 91 (2004) 1092–1103, https://doi.org/10.1111/j.1471-4159.2004.02795.x.
[93] K. Bracey, M. Ju, C. Tian, L. Stevens, D. Wray, Tubulin as a binding partner of the heag2 voltage-gated potassium channel, J. Membr. Biol. 222 (2008) 115–125, https://doi.org/10.1007/s00232-008-9104-x.
[94] P. Enyedi, I. Veres, G. Braun, G. Czirjak, Tubulin binds to the cytoplasmic loop of TRESK background K^+ channel in vitro, PloS One 9 (2014), e97854, https://doi.org/10.1371/journal.pone.0097854.
[95] S.F. Hamm-Alvarez, M.P. Sheetz, Microtubule-dependent vesicle transport: modulation of channel and transporter activity in liver and kidney, Physiol. Rev. 78 (1998) 1109–1129, https://doi.org/10.1152/physrev.1998.78.4.1109.
[96] L. Hedstrom, IMP dehydrogenase: structure, mechanism, and inhibition, Chem. Rev. 109 (2009) 2903–2928, https://doi.org/10.1021/cr900021w.
[98] K. Yamano, D. Ishikawa, M. Esaki, T. Endo, The phosphate carrier has an ability to be sorted to either the TIM22 pathway or the TIM23 pathway for its import into yeast mitochondria, J. Biol. Chem. 280 (2005) 10011–10017, https://doi.org/10.1074/jbc.M413264200.
[99] Y. Kang, L.F. Fielden, D. Stojanovski, Mitochondrial protein transport in health and disease, Semin. Cell Dev. Biol. 76 (2018) 142–153, https://doi.org/10.1016/j.semcdb.2017.07.028.
[100] W. Wang, X. Chen, L. Zhang, J. Yi, Q. Ma, J. Yin, W. Zhuo, J. Gu, M. Yang, Atomic structure of human TOM core complex, Cell Discovery 6 (2020) 67, https://doi.org/10.1038/s41421-020-00198-2.
[101] S. Callegari, L.D. Cruz-Zaragoza, P. Rehling, From TOM to the TIM23 complex – handing over of a precursor, Biol. Chem. 401 (2020) 709–721, https://doi.org/10.1515/hsz-2020-0101.
[102] N. Pfanner, B. Warscheid, N. Wiedemann, Mitochondrial proteins: from biogenesis to functional networks, Nat. Rev. Mol. Cell Biol. 20 (2019) 267–284, https://doi.org/10.1038/s41580-018-0092-0.
[103] A. Pierleoni, P.L. Martelli, P. Fariselli, R. Casadio, BaCelLo: a balanced subcellular localization predictor, Bioinformatics 22 (2006) e408–e416, https://doi.org/10.1093/bioinformatics/btl222.
[104] W.W.L. Cheng, N. D'Avanzo, D.A. Doyle, C.G. Nichols, Dual-mode phospholipid regulation of human inward rectifying potassium channels, Biophys. J. 100 (2011) 620–628, https://doi.org/10.1016/j.bpj.2010.12.3724.
[105] H.H. Liou, S.S. Zhou, C.L. Huang, Regulation of ROMK1 channel by protein kinase a via a phosphatidylinositol 4,5-bisphosphate-dependent mechanism, Proc. Natl.

Acad. Sci. U. S. A. 96 (1999) 5820–5825, https://doi.org/10.1073/pnas.96.10.5820.
[106] Y. Comoglio, J. Levitz, M.A. Kienzler, F. Lesage, E.Y. Isacoff, G. Sandoz, Phospholipase D2 specifically regulates TREK potassium channels via direct interaction and local production of phosphatidic acid, Proc. Natl. Acad. Sci. U. S. A. 111 (2014) 13547–13552, https://doi.org/10.1073/pnas.1407160111.
[107] C.V. Robinson, T. Rohacs, S.B. Hansen, Tools for understanding nanoscale lipid regulation of ion channels, Trends Biochem. Sci. 44 (2019) 795–806, https://doi.org/10.1016/j.tibs.2019.04.001.
[108] D.W. Hilgemann, Local PIP(2) signals: when, where, and how? Pflugers Arch. 455 (2007) 55–67, https://doi.org/10.1007/s00424-007-0280-9.
[109] D. Tran, P. Gascard, B. Berthon, K. Fukami, T. Takenawa, F. Giraud, M. Claret, Cellular distribution of polyphosphoinositides in rat hepatocytes, Cell. Signal. 5 (1993) 565–581, https://doi.org/10.1016/0898-6568(93)90052-N.
[110] A. Yoshida, H. Hayashi, K. Tanabe, A. Fujita, Segregation of phosphatidylinositol 4-phosphate and phosphatidylinositol 4,5-bisphosphate into distinct microdomains on the endosome membrane, Biochim. Biophys. Acta Biomembr. 1859 (2017) (1880-1890), https://doi.org/10.1016/j.bbamem.2017.06.014.
[111] P.A. Welling, ROMK and Bartter Syndrome Type 2, Ion Channels and Transporters of Epithelia in Health and Disease, Physiology in Health and Disease, Springer, New York, NY, 2016, pp. 643–658.
[112] R. Westland, M. Bodria, A. Carrea, S. Lata, F. Scolari, V. Fremeaux-Bacchi, V. D. D'Agati, R.P. Lifton, A.G. Gharavi, G.M. Ghiggeri, S. Sanna-Cherchi, Phenotypic expansion of DGKE-associated diseases, J. Am. Soc. Nephrol. 25 (2014) 1408–1414, https://doi.org/10.1681/ASN.2013080886.
[113] D. Gimelreich, M.M. Popovtzer, H. Wald, G. Pizov, Y. Berlatzky, D. Rubinger, Regulation of ROMK and channel-inducing factor (CHIF) in acute renal failure due to ischemic reperfusion injury, Kidney Int. 59 (2001) 1812–1820, https://doi.org/10.1046/j.1523-1755.2001.0590051812.x.
[114] Z. Wang, Z. Zhou, Y. Zhang, F. Zuo, J. Du, M. Wang, M. Hu, Y. Sun, X. Wang, M. Liu, Y. Zhang, W. Tang, F. Yi, Diacylglycerol kinase epsilon protects against renal ischemia/reperfusion injury in mice through Krüppel-like factor 15/klotho pathway, Ren. Fail. 44 (2022) 902–913, https://doi.org/10.1080/0886022X.2022.2079524.
[115] G. Traczyk, A. Hromada-Judycka, A. Świątkowska, J. Wiśniewska, A. Ciesielska, K. Kwiatkowska, Diacylglycerol kinase-ε is S-palmitoylated on cysteine in the cytoplasmic end of its N-terminal transmembrane fragment, J. Lipid Res. (2023), 100480. https://doi.org/10.1016/j.jlr.2023.100480. Epub ahead of print. PMID: 38008259.
[116] J. Wang, K. Papanicolaou, R. Tryon, J. Sangalang, B. Salazar, A. Suarez-Pierre, J. Dong, A. Lee, E. Larson, S. Holmes, B. O'Rourke, C. Nichols, J. Lawton, Kir1.1 and SUR1 are not implicated as subunits of an adenosine triphosphate-sensitive potassium channel involved in diazoxide cardioprotection, JTCVS Open 15 (2023) 231–241, https://doi.org/10.1016/j.xjon.2023.06.004. PMID: 37808059; PMCID: PMC10556815.
[117] W. Jennings, S. Doshi, P.K. Hota, A. Prodeus, S. Black, R.M. Epand, Expression, purification, and properties of a human arachidonoyl-specific isoform of diacylglycerol kinase, Biochemistry 56 (9) (2017) 1337–1347, https://doi.org/10.1021/acs.biochem.6b01193. Epub 2017 Feb 24. PMID: 28199087.